The Extraordinary 'Superthin' Spiral Galaxy UGC 7321. I. Disk Color Gradients and Global Properties from Multiwavelength Observations

L. D. Matthews[1,4,5]

J. S. Gallagher, III[2,4,5]

W. van Driel[3,4,5]

ABSTRACT

We present B- and R-band optical imaging and photometry, Hα narrow-band imaging, near-infrared H-band imaging, and H I 21-cm spectroscopy of the nearby (V_h=407 km/s), Sd spiral galaxy UGC 7321. UGC 7321 exhibits a remarkably thin stellar disk with no discernible bulge component. The galaxy has a very diffuse, low surface brightness disk, which appears to suffer relatively little internal extinction in spite of its nearly edge-on geometry ($i \approx 88°$). If seen face-on, UGC 7321 would have an observed central B-band surface brightness of only $\sim$23.4 mag arcsec^{-2}.

The UGC 7321 disk shows significant $B-R$ color gradients in both the radial and vertical directions: $\Delta(B-R) \geq 0.80$ magnitudes along the galaxy major axis, and $\Delta(B-R)$ as large as 0.45 magnitudes is observed parallel to the galaxy minor axis. These color gradients cannot be explained solely by dust and are indicative of changes in the mix of stellar ages and/or metallicity as a function of both radius and height above the galaxy plane. The outer regions of the UGC 7321 disk are too blue to be explained by low metallicity alone ($B-R \leq 0.6$), and must be relatively young. However, the galaxy also contains stellar populations with $B-R > 1.1$, indicating it is not a young or recently-formed galaxy.

The disk of UGC 7321 is not a simple exponential, but exhibits a light excess at small radii, as well as distinct surface brightness zones. Despite its organized disk structure, many of the global properties of UGC 7321 ($M_B = -17.0$; $\mathcal{M}_{HI}$=1.1$\times 10^9 \mathcal{M}_\odot$;

[1]National Radio Astronomy Observatory, 520 Edgemont Road, Charlottesville, VA 22903, Electronic mail: lmatthew@nrao.edu

[2]University of Wisconsin, Department of Astronomy, 475 N. Charter St., Madison, WI 53706-1582

[3]Unité Scientifique Nançay, CNRS USR B704, Observatoire de Paris, 92195 Meudon, France

[4]Guest observer at the WIYN Observatory, which is a joint facility of the University of Wisconsin-Madison, Indiana University, Yale University, and the National Optical Astronomy Observatories.

[5]Visiting Astronomer, Kitt Peak National Observatories, which is operated by the Association of Universities for Research in Astronomy, Inc. (AURA) under a cooperative agreement with the National Science Foundation.

$\frac{\mathcal{M}_{HI}}{L_B}$=1.1 $\mathcal{M}_\odot/\mathcal{L}_\odot$; W_{20}=233 km s^{-1}; h_r=2.1 kpc) are reminiscent of a dwarf galaxy. Together the properties of UGC 7321 imply that it is an under-evolved galaxy in both a dynamical and in a star-formation sense.

Subject headings: galaxies: spiral—galaxies: fundamental parameters—galaxies: evolution—galaxies: individual (UGC 7321)

1. Background

Ogorodnikov (1958) and Vorontsov-Vel'yaminov (1967) were among the first to draw attention to a subset of edge-on spiral galaxies with disk axial ratios as extreme as 30:1[6] and having little or no discernable bulge component. Goad & Roberts (1981) dubbed these galaxies "superthins" and recognized that spiral galaxies selected on the basis of their thin stellar disks and extreme axial ratios also tend to possess a variety of other intriguing properties.

For example, Goad & Roberts (1981) discovered that superthins have low emission-line intensity ratios ([N II]/Hα and [N II]/[S II]), which in a modern perspective suggests that superthins are moderate ionization, low metallicity galaxies more like irregulars than spirals in terms of their H II region properties (see also Bergvall & Rönnback 1995). Similar trends were confirmed for larger samples by Karachentsev & Xu (1991) and Karachentsev (1991).

In spite of having "classic" double-horned global H I profiles (e.g., Matthews & van Driel 1999), often superthins exhibit slowly-rising, solid-body rotation curves throughout most or all of their stellar disks (Goad & Roberts 1981; Karachentsev & Xu 1991; Karachentsev 1991; Cox *et al.* 1996; Makarov *et al.* 1997,1998; Abe *et al.* 1999). Such rotation curves are generally characteristic of late-type dwarf and irregular galaxies rather than normal spirals (cf. Casertano & van Gorkom 1991).

Not only are superthins fascinating objects in their own right, but the very nature of these galaxies makes them extremely valuable objects for exploring a variety of fundamental astrophysical problems, ranging from disk formation and evolution scenarios, to the interpretation of high-redshift galaxy populations, to constraining the stability and dark matter contents of disks (e.g., Karachentsev 1989; Zasov *et al.* 1991; Dalcanton & Schectman 1996). In spite of this, to date only a handful of detailed studies of individual superthins have been undertaken (e.g., Gallagher & Hudson 1976; Bergvall & Rönnback 1995; Cox *et al.* 1996; Matthews 1998; Abe *et al.* 1999).

Measurements of the vertical structure and disk color gradients are of particular interest in the case of superthin spirals, as these can provide important clues to their evolutionary history.

[6]These disk axial ratios were measured on blue photographic survey plates; however, we find the axial ratios tend to become less extreme when measured at a fixed isophote on deeper, red-sensitive CCD images. For this reason, measurements of vertical disk scale heights offer a more robust means of quantifying the thickness of edge-on galaxies.

Vertical structure measurements provide vital constraints on disk stability, dynamical heating mechanisms, and dark matter contents (Matthews 1998; Matthews 1999, hereafter Paper II), and when combined with measures of global properties and disk color gradients, information on the star-formation histories and dynamical evolutionary histories of the galaxies can be gleaned.

UGC 7321 is a superthin galaxy ideally suited to such investigations. Since it is nearby (D$\sim$10 Mpc; Matthews *et al.* 1999b), its structure can be reasonably resolved from the ground. In addition, UGC 7321 appears to suffer little from internal extinction (see below), and it is nearly exactly edge-on ($i \approx 88°$), hence projection effects will have a minimal influence on derived vertical structural parameters (e.g., de Grijs, Peletier, & van der Kruit 1997). Finally, the analysis of UGC 7321 is simplified compared with other edge-on spirals due to the absence of a bulge component.

Here we present measurements of the global properties of UGC 7321 based on new multiwavelength observations including B- and R-band imaging and photometry, narrow-band Hα imaging, near-infrared H-band imaging, and H I 21-cm pencil beam spectroscopy. We also examine H I aperture synthesis data obtained by Rots, Roberts, & Goad (private communication). We use our datasets to measure the radial and vertical color gradients in the disk of UGC 7321 (Sect. 3) and briefly discuss what the color gradients reveal about the evolutionary history of this galaxy. In a second paper (Paper II), we present measurements of the vertical scale height of the UGC 7321 disk. There we combine vertical structural measurements with results from the present work in order to further constrain the stability and dynamical history of UGC 7321.

2. Imaging Data

2.1. Near-Infrared Imaging

We obtained near-infrared (NIR) H-band imaging observations of UGC 7321 in May 1997 using IRIM on the 2.1-m telescope at the Kitt Peak National Observatory[7]. IRIM employs a 256×256 HgCdTe NICMOS3 detector with $1\farcs09$ pixels, yielding a field-of-view of $4\farcm6$ per side. The detector has a gain of 10.5 e^-/ADU and a readnoise of $\sim$37 e^- per pixel rms. The observations were taken in the presence of moderate cirrus, hence our H-band data cannot be reliably photometrically calibrated.

We obtained sets of 9 co-added, 20-s exposures of UGC 7321 at each of 35 telescope pointings. To insure accurate flatfielding and sky subtraction, we shifted the galaxy to a different position on the detector before each series of exposures. In addition, interspersed throughout the target observations, we obtained several series of "blank" sky exposures at regions adjacent to the galaxy.

[7]Kitt Peak National Observatory is operated by the Association of Universities for Research in Astronomy, Inc. under contract with the National Science Foundation.

Linearization corrections to the data were made automatically during data acquisition.

Data reduction was accomplished using standard IRAF[8] tasks. To remove the sky background, a median was made of several groups of temporally consecutive object and blank sky exposures. From these, a median-averaged combination of 25 dark frames was subtracted to remove the structure present in the detector dark current. Finally, the dark-corrected sky frame was subtracted from all dark-corrected object frames.

Flatfielding was accomplished by dividing by a night sky flat composed of the median of all dark-corrected sky and object exposures. Lastly, the flatfielded object exposures were aligned and co-added. Our resulting H-band image of UGC 7321 is shown in Fig. 1. Note the striking thinness of the stellar disk and the complete absence of a bulge component even in the NIR. At the disk center, the vertical exponential scale height is only $\sim$140 pc (Paper II)!

Fig. 2 shows the H-band data in the form of a contour map. Because the disk is so thin, the contours have been stretched in the z-direction for clarity. Note that the contours are quite regular, even near the galaxy center, suggesting that there is not significant dust absorption in the H-band.

In Fig. 3 we plot a major axis profile extracted from the H-band data. From this profile, we see that the disk brightness of UGC 7321 falls off somewhat more steeply on the east side (the righthand side of Fig. 3) than on the west side. It is unlikely this can be attributed to internal extinction effects (which should be small at NIR wavelengths), or to flatfield errors (which are quite small in our H-band images), hence this suggests a slight lopsidedness in the stellar disk of UGC 7321.

Arrows overplotted on Fig. 3 denote "zones" between which the slope of the brightness profile change fairly abruptly. These zones can also be seem from visual inspection of both our NIR and the optical images and are an indication that the disk surface brightness of UGC 7321 deviates somewhat from a smooth, exponential distribution (see also Sect. 2.2.3). This makes it difficult to characterize the H-band major axis profile in terms of a single exponential scale length. As shown by Matthews & Gallagher (1997), this phenomenon is common among extreme late-type spiral galaxies, although the effect is generally lost if the light profile is azimuthally averaged. Matthews & Gallagher (1997) suggested these surface brightness zones may be a signature of limited dynamical evolution in some of the smallest and faintest spirals (see also Sect. 2.3.3).

2.2. Optical CCD Imaging and Photometry

[8]IRAF is distributed by the National Optical Astronomy Observatories, which is operated by the Associated Universities for Research in Astronomy, Inc. under cooperative agreement with the National Science Foundation.

2.2.1. Data Acquisition

We obtained photometrically calibrated B- and R-band CCD imaging observations of UGC 7321 in June 1997 using the 3.5-m WIYN[9] telescope at Kitt Peak. In addition, we obtained narrow-band Hα and uncalibrated B-and R-band observations of the galaxy with the WIYN telescope in April 1997.

The direct imaging camera on the WIYN telescope employs a thinned STIS 2048×2048 CCD with $0''.2$ pixels, yielding a field-of-view of $\sim 7'$ per side. The CCD gain was 2.8 e^- per ADU, and readnoise was ~ 8 e^- per pixel rms. Exposure times were $900s$ in B, $600s$ in R, and $1500s$ in Hα. Seeing during both the April and June observations was $\sim 0''.6$ FWHM. The WIYN telescope takes advantage of the best seeing on Kitt Peak through a combination of thermal controls, active optics, and dome ventilation systems. This, combined with the small pixel scale of the WIYN CCD imaging camera, makes WIYN an ideal facility for obtaining the data necessary for detailed studies of disk structure and color gradients of galaxies.

Our CCD images were reduced using standard IRAF tasks. Individual frames were overscan corrected and bias subtracted in the usual manner. Flatfielding was accomplished by dividing by a mean of 5 dome flats taken in the appropriate filter. The WIYN CCD contains a bad column which was corrected in our images by interpolation from the two adjacent columns.

Both the April and the June observations were obtained during dark time. Photometric calibration for the June run was accomplished by monitoring two standard star fields from Landolt (1992) at two different air masses and then applying standard color term corrections to convert from WIYN natural magnitude system to the Landolt system. The total formal dispersion in our WIYN magnitude zero points is ± 0.03 magnitudes; the validity of our transformations was checked via comparisons with other recent WIYN photometric solutions. Errors in the colors are approximately ± 0.02 magnitudes. Sky brightnesses during our observations were $\mu_{B,sky} \sim 22.1$ mag arcsec^{-2} and $\mu_{R,sky} \sim 19.8$ mag arcsec^{-2}.

Our R-band image of UGC 7321 is shown in Fig. 4 & 5. Note the very diffuse, low surface brightness (LSB) appearance of the disk in spite of its edge-on geometry. Several background galaxies are clearly visible through the disk (e.g., Fig. 6), implying internal extinction is low.

2.2.2. Hα Emission

Our continuum-subtracted Hα image of UGC 7321 is shown in Fig. 7. Due to cirrus, we were unable to obtain a flux calibration for this frame. However, qualitatively, this image shows that Hα emission is present out to radii of at least $r = \pm 2'.5$ (where r is the distance from the galaxy

[9]The WIYN Observatory is a joint facility of the University of Wisconsin-Madison, Indiana University, Yale University, and the National Optical Astronomy Observatories.

center measured along the disk major axis in the plane of the sky).

We see in Fig. 7 that the bulk of the Hα emission in UGC 7321 is confined to a region near the disk midplane roughly $4''$ thick, although diffuse emission is clearly visible at z-heights of up to $\pm 8''$ at galactocentric radii $|r| \leq 1'.0$. We note however that there is a relative dearth of emission within a region offset $8''$ to the east of the disk center (Fig. 8). This "gap" is $\sim 8''$ wide and contains faint plumes of emission extending to $z \geq \pm 7''$ out of the galaxy plane. We also see marginal evidence of several other thin filaments which are more extended in z-height. Deeper narrow-band images are clearly needed to establish whether the central Hα feature could be a signature of blowout from the disk, and whether UGC 7321 may indeed contain a diffuse, ionized medium extended to large z-heights, analogous to that seen in more luminous edge-on spirals (cf. Dettmar 1995 and references therein).

2.2.3. Surface Photometry

We performed surface photometry on UGC 7321 using routines from the IRAF STSDAS analysis package. With the "ellipse" program, we fit a series of 9 concentric ellipses to the UGC 7321 images. Position angle and ellipticity of the ellipses were determined from the outermost galaxy isophotes and were kept fixed throughout the fitting. The galaxy center was chosen to be the position of peak brightness; this location was identical in the B and R (and H) frames. Foreground stars, cosmic rays, and background galaxies within the aperture were removed via background interpolation using the IRAF task "imedit". Sky values were determined by measuring the sky counts in each of several rectangular apertures at various locations on the image (see Matthews & Gallagher 1997).

Because UGC 7321 is so close to edge-on, elliptical apertures are not ideal fits to the galaxy isophotes. Nonetheless, these apertures allow us to measure aperture magnitudes and colors for UGC 7321, and permit an estimate of the mean exponential scale length of its disk. Although the ellipticity of the fitted isophotes is an unreliable method of determining the inclination of near edge-on galaxies, our derived value ($i \approx 88°$) is consistent with the inclination we estimate from the slight asymmetry of the dust features along the galaxy major axis.

Our derived photometric parameters for UGC 7321 are given in Table 1. Errors for the aperture magnitude measurements were computed following Matthews & Gallagher (1997) and take into account sky, flatfield and Poisson errors, as well as the scatter in the photometric solution. Large-scale flatfield errors are the dominant source of uncertainty; the maximum amplitude of the flatfield variations was $\sim$1% of sky in both B and R. Our aperture magnitudes are in good agreement with previous photoelectric values reported by Tully (1988; m_B=13.86) and de Vaucouleurs & Longo (1988; m_R=12.99).

Fig. 9 shows our azimuthally averaged B-band radial surface brightness profile of UGC 7321. Although we noted in Sect. 2.1 that the disk of UGC 7321 is slightly lopsided and shows deviations

from a perfect exponential, an azimuthally-averaged brightness profile permits determination of a "mean" scale length which is useful for offering a global characterization of the size scale of the disk.

Because UGC 7321 is viewed close to edge-on, one must take into account projection effects in analyzing the projected light profile and in deriving an exponential scale length. For a disk with an exponential radial brightness distribution viewed exactly edge-on ($i = 90°$), the projected radial brightness profile along the galaxy midplane (z=0) is expressed as

$$L(r) = L_0(r/h_r)K_1(r/h_r) \tag{1}$$

where K_1 is the modified Bessel function of first order (e.g., van der Kruit & Searle 1981). At small radii ($r/h_r << 1$), this expression can be approximated as

$$L(r) \approx L_0[1 + (r^2/2h_r^2)\ln(r/2h_r)]. \tag{2}$$

Note this implies a slight flattening of the light profile will be observed at small radii compared with a simple, unprojected e^{-r/h_r} function. At large radii ($r/h_r >> 1$), one can write

$$L(r) \approx L_0(\pi r/2h_r)^{1/2}\exp(-r/h_r) \tag{3}$$

(see van der Kruit & Searle 1981). Because of the $\sqrt{r}$ term, this produces a slightly less steep light profile than a pure exponential function with the same scale length. As a result, a scale length derived from fitting a simple, unprojected exponential profile to an edge-on disk will be overestimated. At $r = 2\text{-}3h_r$ this effect is ∼10% (e.g., van der Kruit & Searle 1981).

To derive the scale length for UGC 7321, we have fitted a model projected exponential light profile to our data. Our model is overplotted on Fig. 9. For the purpose of deriving a scale length, the slight deviation of UGC 7321 from the edge-on ($i = 90°$) case is not significant. From our fit we derive a scale length of $h_{r,B}$=44″ ± 2 (compared with $h_{r,B}$=51″ ± 5″ we derive from simply fitting the function $L(r) = L_0e^{-r/h_r}$ to the disk at intermediate r).

A comparison between the data and our model (Fig. 9) shows that in spite of lacking a bulge component, UGC 7321 exhibits a light excess at small radii compared with the prediction of an exponential disk. The B-band *measured* central surface brightness of UGC 7321 (before correction to a face-on value) is 21.6 mag arcsec^{-2}, while that predicted from extrapolation of the exponential fit to small r is ∼0.35 magnitudes fainter. Interestingly, this excess is even more pronounced in the R-band and appears to correspond to a distinct region in the color map of UGC 7321 (see Sect. 3). This strengthens the suggestion that UGC 7321 appears to have a multi-component disk that is more complex than a simple, pure exponential (see also Sect. 2.1). In addition, we note that at $r > 120''$ our observed light profile falls off faster than the projected exponential model, suggesting the stellar disk of UGC 7321 may be truncated (cf. Barteldrees & Dettmar 1994). However, this latter trend should be confirmed with deeper observations on a wide-field CCD where sky subtraction and flatfielding can be accomplished with greater accuracy.

2.2.4. Discussion: The LSB Nature of UGC 7321

For an optically thin disk which is exponential in both the r and z directions, and which is observed inclined at 90°, the face-on central surface brightness will be h_z/h_r times the observed edge-on value. Here h_z is the exponential scale height (cf., van der Kruit & Searle 1981). Transformations from observed surface brightness values to face-on values at other radii may be derived from Equations 1-3 above. Using a thin-disk approximation (see the Appendix) we have derived the additional corrections to these values required for the case where a is disk observed at an inclination slightly less than 90°. After also taking into account internal extinction corrections (see Sect. 3.2.2), we then find that if projected to face-on, the disk of UGC 7321 would have an *observed* B-band central surface brightness of ∼23.4 mag arcsec^{-2}, an extrapolated central surface brightness of ∼23.8 mag arcsec^{-2}, and a mean total disk surface brightness $\bar{\mu}_B$ ∼27.6 mag arcsec^{-2}. Thus UGC 7321 is a very LSB galaxy, and much of its disk would likely be nearly invisible if viewed closer to face-on. As shown below, the internal extinction in UGC 7321 appears to be quite low, thus its LSB appearance must result from a rather low current star formation rate.

Further evidence that the seemingly "anemic" nature of UGC 7321 is due to minimal current star formation comes from comparing its blue luminosity to its far-infrared luminosity. Using the *IRAS* 60μm and 100μm fluxes for UGC 7321 from the NED database and Sage (1993), respectively, and following the prescription of Rice *et al.* (1988), we derive L_{FIR}=7.8×10$^7\mathcal{L}_\odot$, a value nearly two orders of magnitude fainter than the mean for Scd/Sd spirals in the UGC catalogue (Roberts & Haynes 1994). Using our blue luminosity (corrected for internal extinction), we find that L_{FIR}/L_B ≈0.08 for UGC 7321. A comparison with Rice *et al.* (1988) reveals that such low L_{FIR}/L_B ratios are commonly found only in two classes of galaxies: (1) old, red early-type spirals, dE's and S0's with few young stars; (2) gas-rich, extreme late-type spirals with diffuse, extremely LSB disks. Examples of the latter group of objects include the nearby galaxies NGC 4395 (Sd IV), NGC 45 (Sdm IV), and IC 2574 (Sm IV-V). All three of these galaxies have $L_{FIR}/L_B \leq$0.10, $\frac{\mathcal{M}_{HI}}{L_B}$>1, blue optical colors, and highly transparent disks (e.g., Sandage 1961; Matthews *et al.* 1999a).

3. Color Maps

Using our B- and R-band WIYN data, we have produced a $B-R$ color map of UGC 7321 (Fig. 10). A variety of structure is evident in this map, including significant $B-R$ color gradients in both the vertical and radial directions. We discuss these features in detail below.

The global $B-R$ color of UGC 7321 is 0.99, as measured within the outermost observed isophote (25.2 mag arcsec^{-2} in B before correction for inclination), and after correction for Galactic foreground extinction. This $B-R$ color is a typical value for a normal, late-type spiral (cf. Lauberts & Valentijn 1988; de Blok, van der Hulst, & Bothun 1995). This suggests that in spite of its edge-on geometry, the disk of UGC 7321 does not suffer severely from internal

reddening due to dust. We return to this issue below.

3.1. The Nuclear Region of UGC 7321

Near the center of the UGC 7321 disk, our color map reveals a small, very red ($B-R \approx 1.5$) nuclear feature, only a few arcseconds across (Fig. 10). This feature is offset $\sim 5''$ to the east of the disk center as determined from the brightness peak of the R- and B-band images. One possibility is that we are seeing the signature of an embedded nucleus. However, although compact star cluster nuclei are common in late-type low-luminosity spirals with diffuse, LSB disks (Matthews & Gallagher 1997; Matthews *et al.* 1999a), we do not see any direct evidence of such a feature in UGC 7321 in either our WIYN images or in images obtained with the *Hubble Space Telescope* (Matthews *et al.* 1999b). Nonetheless, the location of the compact red feature in the $B-R$ color map is near to that of the peculiar Hα emission features shown in Fig. 8. The optical longslit spectrum of UGC 7321 obtained by Goad & Roberts (1981) also shows a possible kinematic disturbance in the Hα emission at this location. These are hints that some interesting physical processes are at work near the center of the UGC 7321 disk. Further investigation of this region via high resolution spectroscopy, deep Hα imaging, and NIR colors may be fruitful.

Surrounding the compact red feature, our color maps reveal a more extended red region ($B-R \sim 1.2$), visible to $r \approx \pm 20''$ on either side of the disk center and showing a rather abrupt boundary (see also below). Intriguingly, the extent of this region corresponds very closely to the region over which we observe a light excess over a pure exponential disk fit (Sect. 2.2.3). This raises the possibility that this red central region might possibly represent an ancient central starburst, the core of the original protogalaxy, or perhaps even a kinematically distinct disk subsystem analogous to the bulge of normal spirals.

3.2. Radial Color Gradients

3.2.1. General Trends

Cutting into the red central region discussed above are thin blue bands of stars visible along the midplane of the galaxy. These bands grow both thicker and bluer with increasing distance from the galaxy center. At $|r| = 20''$, this layer has $B-R \approx 1.05$, reaching $B-R \approx 0.85$ at $|r| = 1\farcm0$, $B-R \approx 0.80$ at $|r| = 1\farcm5$, $B-R \approx 0.45 \pm 0.10$ at $r = 2\farcm7$, and $B-R \approx 0.55 \pm 0.10$ at $r = -2\farcm7$. Thus, from the nuclear region (where $B-R \approx 1.5$) to the outer disk edge we see a total $B-R$ color change of up to 1.05 magnitudes along the major axis of UGC 7321. This is illustrated in Fig. 11$a-d$, which shows $B-R$ color profiles of UGC 7321 extracted along the major axis, as well as $1\farcs6$ north (through the red nuclear feature), $1\farcs2$ south, and $4\farcs6$ south relative to the major axis, respectively. The extracted profiles were averaged over 12-pixel-wide strips and then

smoothed, hence the red color of the compact red central disk feature is slightly subdued in the profiles shown in Fig. 11. Because we are interested in accurately measuring colors in the faintest regions of the outer disk, we extracted our color profiles from our our uncalibrated B and R images, which have slightly superior flatfields to our photometrically-calibrated data; maximum amplitude variations of the flatfields are $\sim$1% of the sky in B and $\sim$0.5% of the sky in R. We then used comparisons between high signal-to-noise inner disk regions to calibrate the absolute colors from the photometrically-calibrated images. The maximum uncertainties expected from the combination of sky subtraction and flatfield errors are overplotted as dotted lines on Fig. 11. Although signal-to-noise in the outer disk is low, the profiles extracted at all four positions parallel to the major axis show regions with $B-R \leq 0.60$, suggesting these blue outer disk colors are real.

Finally, we draw attention to the presence of a faint, thicker, but highly flattened disk of unresolved stars visible in our color map surrounding the UGC 7321 disk at $|r| \leq 2\farcm0$. This component has $B-R \approx 1.1$ and shows little change in color with galactocentric distance (Fig. 12). Based upon the observations of Galactic globular clusters (see Secker 1995), old, metal-poor stellar populations are expected to have $B-R > 0.8$, hence the highest z-height stars in UGC 7321 appear to represent an "old disk" population (see also below).

3.2.2. Gauging the Effects of Dust

Bluing as a function of increasing galactocentric distance is a well-known feature of spiral galaxy disks (e.g., de Jong 1996). De Jong (1996) has demonstrated through Monte Carlo simulations that in face-on spirals, this observed radial bluing generally cannot be accounted for by dust. He shows that for realistic models, dust creates color gradients of less than 0.3 magnitudes in $B-R$, and argues instead that the observed radial color changes in spirals are indicative of star formation progressing radially outwards in disks over time, leading to stellar age and metallicity gradients. This picture is consistent with a number of semi-analytic galaxy formation models where galaxy disks are built "from the inside out" (e.g., White & Frenk 1991; Mo *et al.* 1998). Nonetheless, the radial color gradient we observe in UGC 7321 ($\Delta B-R \sim 1$) is significantly larger than typical gradients in the de Jong sample (where typically $\Delta B-R \sim 0.6$ magnitudes, even when bulge light is included). Moreover, in most spirals observed edge-on, radial color gradients are generally found to be small (e.g., Sasaki 1987; Aoki *et al.* 1991; Wainscoat, Freeman, & Hyland 1989; Bergvall & Rönnback 1995) or negligible (e.g., Hamabe *et al.* 1980; Jensen & Thuan 1982; de Grijs 1998).

Unfortunately, in edge-on spiral galaxies, color gradients become more difficult to interpret physically, particularly since internal extinction can be quite significant near the galactic plane. The net effect can be both an alteration in the galaxy luminosity profile, and a reddening of the observed optical colors which can vary as a function of r and z. Therefore in order to determine what fraction of the color gradients we observe in UGC 7321 are due to true age and/or metallicity gradients, we must include an assessment of the role of dust in this galaxy.

In practice, accurately quantifying the effects of dust on the observed colors and luminosity distribution in a galaxy is a complicated problem (e.g., de Jong 1996; Xilouris *et al.* 1999). Moreover, standard assumptions about the nature and distribution of dust in normal giant spirals are unlikely to be applicable to low-metallicity LSB galaxies (cf. Han 1992). As a result, the effects of internal extinction in a given galaxy are ideally derived using a combination of sophisticated radiative transfer models and empirical measurements (e.g., Xilouris *et al.* 1999). Such modelling beyond the scope of the present work, so here we derive some fundamental constraints on the effects of dust in UGC 7321 using a very simple model.

Although some authors have argued that the internal extinction in LSB galaxies may be almost negligible (e.g., McGaugh 1994; Tully *et al.* 1998), these claims have only rarely been tested in edge-on systems (e.g., Goad & Roberts 1981; Kodaira & Yamashita 1996; Bergvall & Rönnback 1995; Karachentsev 1999). We have already mentioned several lines of evidence that the internal extinction in UGC 7321 is low (regularity of the H-band isophotes; visibility of background galaxies through the disk; low L_{FIR}/L_B ratio; correspondance between the galaxy center in H- and B-band). Nonetheless, visible inspection of our WIYN images shows the galaxy is clearly not completely devoid of dust, and a number of individual clumps (possibly molecule-rich dark clouds) can be seen in our optical images (e.g., Fig. 5; see also Matthews *et al.* 1999b). In spite of this, the fact that we resolve many of these individual dust clumps instead of seeing a uniform dust lane implies that the disk of UGC 7321 is not optically thick.

Another test of the optical thickness of the UGC 7321 disk comes from a comparison between its optical rotation curve (derived from longslit spectroscopic measurements of Hα emission from H II regions), with a rotation curve derived from H I measurements. From optical longslit measurements, Goad & Roberts (1981) found UGC 7321 to have a slowly rising, solid-body rotation curve throughout much of its stellar disk. If a galaxy disk is optically thick, the rotation curve may appear solid body regardless of its intrinsic shape, as an artifact of one's inability to observe H II regions at small galactocentric radii (Goad & Roberts 1981; Byun 1993). However, a rotation curve of UGC 7321 derived from H I aperture synthesis measurements (Sect. 4.2) confirms that the slow rise of the rotation curve throughout the stellar disk is indeed intrinsic (see Fig. 19, discussed below). Once again we conclude the disk of UGC 7321 is not optically thick.

Dust affects the color and luminosity profiles of galaxies through both the scattering and absorption of optical photons. However, the maximum color change (i.e., maximum reddening) occurs in the pure extinction case. In addition, Byun, Freeman, & Kylafis (1994) have shown that scattering effects become decreasingly important with increasing inclination (see also Bianchi, Ferrara, & Giovanardi 1996). Since here we are primarily interested in estimating the effects of dust on the color gradient, and since we are in the optically thin regime, we can simplify the problem by considering a model of extinction due to a foreground dust screen (see Disney, Davies, & Phillips 1989). For a given amount of dust, the Screen model produces more reddening than a more realistic model of stars mixed with dust, hence it establishes an upper limit to $E(B-R)$ as a function of radius.

To evaluate $E(B-R)$, we begin by attempting to attribute as much of our observed color gradient as possible to dust. We further assume that, to first order, dust extinction in the H-band is negligible (e.g., Fig. 2). In the case of zero intrinsic radial color gradient, a dust-free version of UGC 7321 would exhibit no radial color gradient in $R-H$, hence we can use the changes we do observe in the $R-H$ color to estimate the amount of extinction at a given radius. We do not attempt to reproduce the clumpy nature of the dust in our model (which again, would decrease any reddening effects), but assume the dust distribution is roughly exponential in the radial and vertical directions (e.g., Wainscoat, Freeman, & Hyland 1989; Xilouris *et al.* 1999). In this case the extinction along an interval from r to δr can be expressed as

$$\delta A_{\lambda,i}(r,z) = \begin{cases} A_{\lambda,0} e^{(-r/h_{r,d} - |z|/h_{z,d})} \delta r & r \leq R_{max} \\ 0 & r > R_{max} \end{cases} \quad (4)$$

where $A_{\lambda,0}$ is the absorption in magnitudes per unit length at a given wavelength, $r = R_{max}$ corresponds to the edge of the stellar disk, $h_{r,d}$ is the scale length of the dust, and $h_{z,d}$ is the scale height of the dust (see also Wainscoat, Hyland, & Freeman 1989).

Fig. 13 shows a plot of the "pseudo" $R-H$ color profile of UGC 7321 along the major axis interval r=0–120″. Here the R-band data were smoothed to match the resolution of the H-band observations. Because our H-band data are not photometrically-calibrated, we have chosen an arbitrary normalization such that our "pseudo" $R-H$ color is 0 near r=80″. In Fig. 13, we see that near r=0, the R-band light is depressed by roughly 40% relative to the H-band, corresponding to an R-band extinction $A_{R,0} \approx$0.55 magnitudes per kiloparsec. Assuming the extinction law of Bouchet *et al.* (1985), we derive $A_{B,0}$=0.89 magnitudes per kiloparsec.

From Fig. 13 we estimate a scale length of the dust distribution of $h_{r,d} \approx$40″, which appears consistent with the observed dust distribution in our images. Although in giant spirals, it is often assumed the dust has a similar scale length to the old stellar disk (e.g., Kylafis & Bahcall 1987), or even extends beyond it (e.g., Xilouris *et al.* 1999), this does not appear to hold in UGC 7321. We see an abrupt end to the presence of resolved dust clumps beyond radii $|r| \approx 80''$ in both our WIYN images, and in *Hubble Space Telescope* images obtained by Matthews *et al.* (1999b). Moreover, background galaxies are readily visible through the UGC 7321 disk beyond these radii (Matthews *et al.* 1999b), implying extinction has dropped appreciably. For the vertical scale height of the dust, we adopt $h_{z,d}$=2″.3, which is half the scale height of the old stellar disk (Sect. 3.3; see also Paper II).

Using Equation 4, we can now derive an extinction-corrected $B-R$ color profile for UGC 7321 along its major axis (Fig 14*a*) and offset 1″.6 to the north (Fig 14*b*). We see that even the extinction-corrected radial color gradient remains pronounced ($\Delta B-R \sim 0.80$ mag). This demonstrates that *a significant fraction of the observed radial color gradient in UGC 7321 appears to be due to stellar population and/or metallicity gradients.*

3.2.3. Discussion and Interpretation

The presence of the observed radial disk color gradients in UGC 7321 has several implications. Regions with $B-R<0.8$ are too blue to be accounted for by old, metal-poor stellar populations (e.g., Secker 1995), but instead must result from a mixture of ages. Without resolving these populations, we cannot uniquely constrain the mix of stars present. However, the bluest colors we reliably measure in UGC 7321 ($B-R<0.6$) are comparable, for example, to young regions in the moderate metallicity giant Magellanic galaxy NGC 4449 (Bothun 1986) and to the predicted colors of the younger outer regions of a smoothly evolving galaxy with a high halo spin parameter and an age of ∼10 Gyr, as in the models of Jimenez *et al.* (1998). In either case, it is likely that youthful stars are a significant contributor to the blue colors of the outer disk of UGC 7321 (see also Bell *et al.* 1999). This assertion is strengthened by the presence of Hα emission in the outer disk (Fig. 7) and the existence of resolved supergiant stars at these radii (Matthews *et al.* 1999b).

We note that edge-on, superthin LSB galaxies like UGC 7321 are especially valuable for studies of the outer regions of disks, as they may contain some of the most pristine, unevolved galaxian disk environments observable in the nearby universe. However, because these disk regions are so optically thin, they would become very difficult to detect in galaxies viewed at lower inclinations. For example, if viewed near face-on, the portions of the UGC 7321 disk where $B-R \leq 0.6$ would have an observed B-band surface brightnesses of only $\geq$27.6 mag arcsec^{-2}. Such faintness levels are only rarely reliably achieved in galaxy imaging surveys due to combinations of short integration times, scattered light, limited detector fields-of-view, and flatfield uncertainties (cf. Morrison, Boronson, & Harding 1994; Lequeux *et al.* 1996).

In spite of the potentially very young outer disk regions of UGC 7321, its moderately red central disk (where $B-R \approx 1.2$) and its somewhat thicker "old disk" (where $B-R \approx 1.1$) both indicate that UGC 7321 is likely to contain stellar populations with ages in excess of 10 Gyr (see Jimenez *et al.* 1998). As demonstrated above, accounting for a reasonable amount of reddening due to dust does not affect this conclusion. The red stellar components in UGC 7321 imply that this is not a young galaxy presently undergoing its first epoch of star formation.

Our observed colors and color gradients in UGC 7321 are similar to those found in other LSB spirals by de Blok, van der Hulst, & Bothun (1995; see also Impey & Bothun 1997). A consistent model for UGC 7321 is then that of a disk galaxy which has made stars slowly and is now seen to be under-evolved relative to typical giant spirals (see also O'Neil *et al.* 1997; Jimenez *et al.* 1998). This would account for the low gas metallicity of UGC 7321 (Goad & Roberts 1981), the large H I mass fraction (Sect. 4), and the low density of stars (i.e., the low optical surface brightness disk). Thus while LSB disks like UGC 7321 may be *unevolved* galaxies, we concur with the suggestion of Jimenez *et al.* (1998) that *LSB galaxies are not necessarily young.*

In order to preserve its relatively strong radial color gradients over many Gyr, it appears that viscous evolution in the disk of UGC 7321 has been minimal. In giant spirals, viscous evolution (which redistributes angular momentum in the disk) is often argued to be responsible for the

relatively smooth exponential luminosity profiles of most disk galaxies (e.g., Lin & Pringle 1987). This process is also expected to partially smooth color gradients due to stellar age and metallicity changes with radius (e.g., Firmani, Hernández, & Gallagher 1996). However, such a mechanism may not be able to work efficiently in galaxies like UGC 7321, due to both the low disk surface density (which considerably extends dynamical timescales) and the slowly rising rotation curve [which produces limited shear in the inner disk regions (Lin & Pringle 1987; see also Matthews & Gallagher 1997)]. The gradients in the H-band major-axis profile of the UGC 7321 disk (Sect. 2.1) and the deviation of the azimuthally-averaged profile from a pure exponential disk at small r (Sect. 2.2.3) may be additional signs that viscous evolution has been limited in this galaxy compared with normal spirals.

Finally, we note that at intermediate galactic radii, the eastern side of UGC 7321 has a slightly bluer mean color than the western side. This result is insensitive to reasonable sky subtraction and flatfield errors. One explanation could be that we are seeing the projection of a spiral arm(s), although it remains uncertain how much spiral structure a thin disk like UGC 7321 might actually sustain, since spiral structure is believed to be an efficient disk heating mechanism (e.g., Lacey 1991 and references therein). Moreover, at least some self-gravity is needed for spiral arm formation, but if the disk of UGC 7321 were completely self-gravitating, it would be highly unstable to "firehose" instabilities and hence to vertical thickening (Zasov, Makarov, & Mikailova 1991; Matthews 1998). An alternative is that there are asymmetries in the stellar distribution of UGC 7321 due to patchy star-formation (see also Gerritsen & de Blok 1999).

3.3. Vertical Color Gradients

The presence of vertical color gradients in galaxies offers an important clue toward the dynamical evolution of galaxian disks, since such gradients are predicted to occur as a consequence of dynamical heating processes (e.g., Just, Fuchs, & Wielen 1996). Unfortunately, vertical color gradients are very difficult to measure in most edge-on spirals due to dust, contamination from the bulge component, and the effects of atmospheric seeing. To date, only a few analyses of edge-on spirals have uncovered non-negligible vertical color gradients (e.g., Wainscoat, Freeman, & Hyland 1989; Bergvall & Rönnback 1995), while many workers have reported such gradients to be very small or negligible (e.g., Jensen & Thuan 1982; de Grijs, Peletier, & van der Kruit 1997).

Fig. 15*a*-*h* illustrates the vertical color profiles of the UGC 7321 disk at various galactocentric distances. At $r = 0$, we see very little z color gradient: $B - R \sim 1.2$ at a range of z values (Fig. 15*a*), although a slight asymmetry is visible. At $r = 6''$ (Fig 15*b*), we see the addition of a peak with $B - R \sim 1.45$. Note its displacement from the disk midplane; this peak is in the vicinity of the red nuclear feature discussed in Sect. 3.1. At r=10″ (Fig 15*c*), the vertical color gradient is again fairly flat ($B - R \sim 1.2$), with a very slight bluing visible near z=1″.5. At r =0′.5 (Fig 15*d*), the high z regions of the disk have nearly the same color as those at r=0 (this is due to the "old disk" of red stars discussed above), but at small z values, the disk has become much bluer than

at smaller galactocentric radii. Finally, with further increasing radius, while the color at high z continues to stay nearly constant, the color at small z grows increasingly bluer (Fig. 15*e*-*h*), consistent with the radial bluing observed along the major axis of the galaxy in Fig. 11.

Vertical color gradients of the type we observe over much of the disk of UGC 7321 (i.e. redder with increasing z height) are predicted to occur due to dynamical disk evolution in which older stellar populations acquire higher velocity dispersions over time due to heating processes (e.g., Fuchs & Wielen 1987; Just, Fuchs, & Wielen 1996). UGC 7321 represents one of the few examples of this type of vertical color structure being directly observed in a galaxy disk. Thus even the most dynamically cold examples of nearby galaxy disks appear to have undergone some dynamical heating. Nonetheless, the exact mechanism by which older stars are dynamically heated and how they are redistributed as a function time remain uncertain (see review by Lacey 1991) and different mechanisms may operate in different galaxies, depending upon factors like environment, degree of self-gravity, and the size and number of molecular clouds. The relative simplicity of UGC 7321, and its status as a relatively unevolved galaxy make this an ideal system to help place important constraints on these issues. We explore this further in Paper II.

Using the extinction parameters derived in Sect. 3.2.2, we can also estimate the effects of dust reddening on our observed vertical color gradients. We adopt for a scale height of the dust half the scale height of the old stellar disk (Xilouris *et al.* 1999). Using the stellar scale height of the old disk derived in Paper II, this yields $h_{z,d}$=2$''$.3. Fig. 16 shows an example of one of our vertical color profiles corrected for dust reddening. We see that at the galactocentric radii where the vertical color gradients become the strongest, correction for dust reddening acts to slightly increase $\Delta(B-R)$ along the vertical direction.

4. HI Observations

4.1. HI Pencil Beam Mapping

In June 1997 we used the Nançay Decimetric Radio Telescope to obtain a 7-point pencil-beam map of UGC 7321 in the 21-cm line of neutral hydrogen (H I). At the declination of UGC 7321, the Nançay Radio Telescope has a FWHM beam size of approximately 4$'$E-W×23$'$N-S. Other details regarding the Nançay telescope may be found in, e.g., Matthews, van Driel, & Gallagher (1998).

UGC 7321 was observed at 7 different telescope pointings, including a position corresponding to the optical center of the galaxy, and positions offset 2$'$, 4$'$, and 6$'$ east and west of center, respectively. The observations were obtained in total power (position-switching) mode using consecutive pairs of two-minute on- and two-minute off-source integrations. Total integration times were 2-3 hours at each pointing. For these observations, the autocorrelator was divided into two pairs of cross-polarized receiver banks, each with 512 channels and a 6.4 MHz bandpass. This yielded a channel spacing of 2.6 km s^{-1}, for an effective velocity resolution of ∼3.3 km s^{-1}.

Fortuitously, UGC 7321 is oriented along nearly an E-W line, so the Nançay telescope provides sufficient spatial resolution along this direction to obtain crude information about the H I distribution and kinematics of the galaxy. The individual spectra obtained at each telescope pointing are shown in Fig. 17 and the resulting global spectrum in Fig. 18. Note the global profile appears quite symmetric. Table 1 gives our derived global H I parameters. Errors were computed following Matthews, van Driel, & Gallagher (1998). Our values are in good agreement with the recent single-dish H I observations of UGC 7321 obtained by Haynes *et al.* (1998) using the Green Bank 140-ft telescope.

Our Nançay observations show that the H I gas in UGC 7321 clearly extends beyond the optical galaxy, confirming the results of Hewitt, Haynes, & Giovanelli (1983). Significant flux is detected at the pointings both 4′E and 4′W of the galaxy, giving a lower limit for the for H I-to-optical diameter ratio of $D_{HI}/D_{opt} \geq 1.25$. In addition, we detect a small amount of H I flux ($\sim$1.1 Jy km s^{-1}) in our observation 6′W of the galaxy center. From the Nançay data alone, it is difficult to assess whether this flux is due to a sidelobe contamination or real extended emission, since the strength of the Nançay telescope sidelobes varies significantly with the hour angle of the source (Guibert 1973).

4.2. HI Aperture Synthesis Data

After our Nançay observations were obtained, we had the opportunity to examine H I aperture synthesis data of UGC 7321 obtained by Rots, Roberts, & Goad (private communication) using the Very Large Array (VLA). These observations were obtained in C array in 1981 using 18 antennas, hence they do not achieve the same sensitivity limits as modern VLA data, but they still offer a useful complement to our Nançay dataset. Thirty-one independent velocity channels were used for the observations, with a velocity resolution of $\sim$10.3 km s^{-1} per channel. The FWHM beamwidth was $\sim$12″.

Using the VLA data, we derived a position-velocity diagram for UGC 7321. By assuming that at each point along the major axis the maximum velocity traces the rotation, we have derived the rotation curve shown in Fig. 19. This figure confirms the slowly-rising, solid body nature of the rotation of UGC 7321 throughout its stellar disk, as was first seen in the optical rotation curve of Goad & Roberts (1981). Although beam-smearing may be expected to slightly decrease the amplitude of our derived H I rotational velocities, this effect is not expected to exceed a few kilometers per second, or to be significant beyond 2–2.5 beam diameters from the disk center (e.g., Swaters 1999), hence it cannot explain the shallow shape of the inferred rotation curve. Finally, we note that Fig. 19 suggests that the rotation curve of UGC 7321 does not begin to flatten until near the edge of the stellar disk. This is consistent with UGC 7321 being a galaxy whose dynamics are dominated by a dark halo even at small galactocentric radii (e.g., Matthews 1998). However, deeper, more sensitive H I aperture synthesis measurements would be valuable for further constraining the detailed shape of the outer rotation curve.

The integrated H I map of UGC 7321 derived by Rots, Roberts, & Goad (private communication) confirms a slight extension of the H I on the west side of the galaxy compared with the east side, consistent with our Nançay data. It also permitted us to measure an H I diameter of D_{HI} ∼7′.1 for UGC 7321 at the limiting H I column density of the observations ($N_{HI} \sim 7 \times 10^{20}$ atoms cm^{-2}). Thus $D_{HI}/D_{opt} \geq$1.2, in agreement with our Nançay lower limit.

4.3. Discussion

It is somewhat difficult to accurately compare the H I extent of UGC 7321 with other spirals since the commonly-quoted D_{HI}/D_{25} ratio (where D_{25} is measured at a face-on-corrected isophote) in not particularly meaningful for a galaxy like UGC 7321, whose face-on central surface brightness is only ∼ 23.4 mag arcsec^{-2}. Moreover, we cannot unambiguously translate our limiting observed H I column density into an H I surface density due to projection effects, thus it is difficult to accurately measure D_{HI} at some canonical surface density (e.g., 1 $\mathcal{M}_{\odot}$ pc^{-2}).

In terms of optical scale length, the H I in UGC 7321 extends to at least $5.5h_r$. Although this value may increase with more sensitive VLA observations, such an extent is still quite normal for both high and low surface brightness late-type spirals having similar rotational velocities to UGC 7321 (see Fig. 8 of de Blok, McGaugh, & van der Hulst 1996).

If we assume both the stellar and the H I disks of UGC 7321 are optically thin, and hence both similarly enhanced in surface brightness due to their edge-on projection, then we see that the maximum H I extent of the disk relative to the maximum optical extent is typical for Sd spirals (e.g., Hewitt, Haynes, & Giovanelli 1983). We can more directly compare with two other Sd superthins previously mapped in H I: D_{HI}/D_{opt} ∼1.2 was also found by Cox *et al.* (1996) for the superthin spiral UGC 7170 and by Abe *et al.* (1999) for the superthin IC 5249, both at similar limiting H I column densities and optical surface brightnesses.

Ignoring internal extinction effects, the $\frac{\mathcal{M}_{HI}}{L_B}$ ratios of UGC 7321, UGC 7170, and IC5249 are 2.6, 3.4, and 2.3 (in solar units), respectively, and the superthin spiral ESO 146-014 studied by Bergvall & Rönnback (1995) has $\frac{\mathcal{M}_{HI}}{L_B}$∼2.8. If we assume all have internal extinctions similar to UGC 7321 ($A_{B,i} \sim 0.89$ mags; Sect. 3.2.2), the implied $\frac{\mathcal{M}_{HI}}{L_B}$ ratios are still significantly larger than typical values for normal Sd spirals derived by Roberts & Haynes (1994; $\frac{\mathcal{M}_{HI}}{L_B}$∼0.63), although not as extreme as some of the unevolved dwarf galaxies studied by van Zee *et al.* (1995) or some of the extreme late-type LSB spirals in the sample of Matthews & Gallagher (1997) which have $\frac{\mathcal{M}_{HI}}{L_V}$ as high as 10 (see also Salzer *et al.* 1991; Matthews, van Driel, & Gallagher 1998).

Van der Hulst *et al.* (1993) suggested that low gas surface densities are responsible for the low star-formation efficiencies in LSB galaxies (see also de Blok, McGaugh, & van der Hulst 1996; Gerritsen & de Blok 1999). Although we cannot unambiguously recover the radial H I surface density distribution in UGC 7321 due to its edge-on geometry (cf. Olling 1996), we can compute

a mean H I surface density within the stellar disk. Adopting the definition $\overline{\Sigma}_{HI} = \mathcal{M}_{HI}/\pi R_{opt}^2$, where R_{opt} is the linear optical diameter of the disk (e.g., Roberts & Haynes 1994) we find $\overline{\Sigma}_{HI}$=5.3 $\mathcal{M}_\odot$ pc^{-2}. This value is considerably lower than the median of this quantity found by Roberts & Haynes (1994) for Scd/Sd spirals in the UGC catalogue: $\overline{\Sigma}_{HI}$=9.80 $\mathcal{M}_\odot$ pc^{-2}, but is consistent with the $\overline{\Sigma}_{HI}$ ratios of several of the LSB galaxies in the sample of de Blok, McGaugh, & van der Hulst (1996).

5. Summary

We have presented B- and R-band imaging and photometry, near-infrared H-band imaging, narrow-band Hα imaging, and H I 21-cm line measurements of the nearby, edge-on Sd spiral galaxy UGC 7321.

UGC 7321 is a "superthin" galaxy, with an extremely dynamically cold stellar disk and no discernible bulge component, even in the near-infrared. In spite of its edge-on orientation, UGC 7321 is visibly quite diffuse and it is clear that its intrinsic optical surface brightness is quite low. The dust content of UGC 7321 also appears to be small, hence we argue that the "anemic" appearance of the galaxy results from the low-level of current star formation rather than severe internal extinction.

UGC 7321 exhibits significant $B-R$ color gradients in the radial direction: measured from the disk center to its edges edge, $\Delta(B-R)$ ∼1.05 magnitudes along the galaxy major axis. Dust alone cannot explain the large gradient. Using a simple extinction model we find $\Delta(B-R)_{cor}$ ∼0.80 after correction for internal reddening. This is somewhat larger than the color gradients typically observed in normal giant spirals (cf. de Jong 1996), and suggests significant stellar population gradients in the disk of UGC 7321.

The outermost disk regions of UGC 7321 have $B-R \leq$0.6, suggesting they are composed of stellar populations that include a significant fraction of young stars. However, UGC 7321 also contains a population of old stars with $B-R \geq$1.1, indicating it is not a young or recently-formed galaxy. The rather strong radial segregation of these populations suggests that the galaxy has evolved quite slowly and perhaps that viscous evolution has not operated efficiently in this system.

UGC 7321 also exhibits appreciable vertical color gradients: $\Delta B-R$ as large as 0.45 magnitudes was measured parallel to the minor axis. This is a reflection of a concentration of young blue stars along the galaxy midplane, and a population of the older, red stars at larger scale heights. This type of age segregation is predicted to occur due to dynamical heating processes in spiral disks, but UGC 7321 represents one of the few examples of it being directly observed in an external galaxy. This implies that even dynamically cold disks like UGC 7321 have undergone some dynamical heating.

The stellar light distribution of the UGC 7321 disk cannot be characterized by a single

exponential function. A light excess over the prediction of an exponential model is seen at small radii, and in both optical and NIR wavelengths, the disk appears to contain distinct surface brightness "zones" between which the slope of the brightness profile changes. This may be an additional signature of minimal viscous evolution. It also brings into question the prediction of some semi-analytic galaxy models (e.g., Dalcanton, Spergel, & Summers 1997) that exponential stellar disks are a natural product of the disk formation process.

In spite of its regular, organized disk, many of the global properties of UGC 7321, including its luminosity, H I content, rotational velocity, and $\frac{\mathcal{M}_{HI}}{L_B}$ ratio (Table 1), as well as its slowly-rising, solid-body rotation curve (Fig. 19) are more typical of a dwarf irregular galaxy than a normal Sd spiral. The origin of such vastly different disk morphologies in an otherwise similar physical parameter space remains unclear, but it may place an important constraint on galaxy formation and evolution models.

Together the properties of UGC 7321 suggest that it is an under-evolved galaxy in both a dynamical and in a star-formation sense. Nonetheless, this galaxy clearly demonstrates that even seemingly simple "pure disk" galaxies like the superthins are highly complex systems.

We are grateful Arnold Rots and Mort Roberts for providing us with the fully-calibrated VLA H I data of UGC 7321. We also thank Mike Merrill for assistance with the IRIM observations at Kitt Peak and Wanda Ashman for creating the artwork for the Appendix. This research was partially funded by the Wide Field and Planetary Camera 2 (WFPC2) Investigation Definition Team, which is supported at the Jet Propulsion Laboratory (JPL) via the National Aeronautics and Space Administration (NASA) under contract No. NAS7-1260. The Nançay Radio Observatory is the department *Unité Scientifique Nançay* of the *Observatoire de Paris* and is associated with the French *Centre National de Recherche Scientifique* (CNRS) as the *Unité de Service et de Recherche* (USR), No. B704. The Nançay Observatory also gratefully acknowledges the financial support of the *Région Centre* in France. This research made use of the NASA/IPAC Extragalactic Database (NED), which is operated by the Jet Propulsion Laboratory, California Institute of Technology, under contract with the National Aeronautics and Space Administration.

A. Estimating the Effects of Inclination on the Observed Central Surface Brightness of a Disk

When deriving central surface brightness measurements of galaxies, it is desirable to convert measured values to face-on values in order that galaxies observed at different inclinations can be meaningfully compared. However, for highly-inclined galaxies, the approximation that $\mu_{face-on} = \mu_{observed} + 2.5\log(a/b)$ (e.g., Freeman 1970) breaks down, and alternative corrections must be used. Here we derive a simple formula for this purpose, using a "thin disk" approximation.

In our model we assume the galaxy disk is optically thin and has an exponential brightness

profile along the r direction of the form $L(r) = L_0 e^{-r/h_r}$, where L_0 is the luminosity volume density and h_r is the disk scale length. We also assume the disk has a finite but non-negligible thickness of $2h_z$, and a constant brightness along the z direction (see Fig. 20). For such a disk, the central surface brightness if viewed edge-on is expressed as

$$L(0)_{i=90} = L_0 \int_{-\infty}^{+\infty} e^{-r/h_r} dr = 2L_0 h_r; \tag{A1}$$

if viewed face-on, the central surface brightness would be simply $L(0)_{i=0} = 2L_0 h_z$.

Now suppose our model disk is viewed at some arbitrary angle $i' < 90°$ through a line of sight along a vector $\mathbf{x}$ (see Fig. 21). We define i as the angle between the line of sight and a normal to the disk. Now the integrated brightness of the disk along a path from $x = 0$ to $x = x_{max}$ becomes

$$L(0)_{i=i'} = 2L_0 \int_0^{x_{max}} e^{x \sin i / h_r} \sin i \; dx. \tag{A2}$$

Taking the integral, and making the substitution

$$x_{max} = h_z / \cos i, \tag{A3}$$

we find that

$$L(0)_i = 2L_0 h_r [1 - e^{-h_z \tan i / h_r}]. \tag{A4}$$

To apply this approximation to a real galaxy, one can substitute the measured radial and vertical scale heights for h_r and h_z respectively, provided that the conditions $h_z << h_r$ and

$$(90 - i') > \tan^{-1} (h_z / x_{max}) \tag{A5}$$

both hold.

REFERENCES

Abe, F. *et al.* 1999, AJ, 118, 261

Aoki, T. E., Hiromoto, N., Takami, H., & Okamura, S. 1991, PASJ, 43, 755

Barteldrees, A. & Dettmar, R.-J. 1994, A&AS, 103, 475

Bell, E. F., Bower, R. G., de Jong, R. S., Hereld, M., & Rauscher, B. J. 1999, MNRAS, 302, L55

Bergvall, N. & Rönnback, J. 1995, MNRAS, 273, 603

Bianchi, S., Ferrara, A., & Giovanardi, C. 1996, ApJ, 465, 127

Bothun, G. D. 1986, AJ, 91, 507

Bouchet, P., Lequeux, J., Maurice, E., Prévot, L., & Prévot-Burnichon, M. L. 1985, A&A, 149, 330

Burstein, D. & Heiles, C. 1984, ApJS, 54, 33

Byun, Y.-I. 1993, PASP, 105, 993

Byun, Y. I., Freeman, K. C., & Kylafis, N. D. 1994, ApJ, 432, 114

Casertano, S. & van Gorkom, J. H. 1991, AJ, 101, 1231

Cox, A. L., Sparke, L. S., van Moorsel, G., & Shaw, M. 1996, AJ, 111, 1505

Dalcanton, J. J. & Schectman, S. A. 1996, ApJ, 465, L9

Dalcanton, J. J., Spergel, D. N., & Summers, F. J. 1997, ApJ, 482, 659

de Blok, W. J. G., van der Hulst, J. M., & Bothun, G. D. 1995, MNRAS, 274, 235

de Blok, W. J. G., McGaugh, S. S., & van der Hulst, J. M. 1996, MNRAS, 283, 18

de Grijs, R. 1998, MNRAS, 299, 595

de Grijs, R., Peletier, R. F., & van der Kruit, P. C. 1997, A&A, 327, 966

de Jong, R. S. 1996, A&A, 313, 377

Dettmar, R. -J. 1995, in Physics of the Interstellar Medium and the Intergalactic Medium, edited by A. Ferrara, C. F. McKee, C. Heiles, & P. R. Shapiro, ASP Conference Series, Vol. 80, (Astronomical Society of the Pacific, San Francisco), p. 398

de Vaucouleurs, A. & Longo, G. 1988, Catalogue of Visual and Infrared Photometry of Galaxies From 0.5μm to 10μm (1961-1985), University of Texas Monographs in Astronomy No. 5 (Austin, University of Texas at Austin)

Disney, M. J., Davies, J. I., & Phillips, S. 1989, MNRAS, 239, 939

Elmegreen, D. M. & Elmegreen, B. G. 1984, ApJS, 54, 127

Firmani, C. Hernández, X., & Gallagher, J. 1996, A&A, 308, 403

Freeman, K. C. 1970, ApJ, 160, 811

Fuchs, B. & Wielen, R. 1987, in The Galaxy, Proceedings of the NATO Advanced Study Institute, Cambridge, England, edited by G. Gilmore, and R. Carswell, (Reidel, Dordrecht), p.375

Gallagher, J. S. & Hudson, H. S. 1976, ApJ, 209, 389

Gerritsen, J. P. E. & de Blok, W. J. G. 1999, A&A, 342, 655

Goad, J. W. & Roberts, M. S. 1981, ApJ, 250, 79

Guibert, J. 1973, A&AS, 12, 263

Hamabe, M., Kodaira, K., Okamura, S. & Takase, B. 1980, PASJ, 32, 197

Han, M. 1992, ApJ, 391, 617

Haynes, M. P., Hogg, D. E., Maddalena, R. J., Roberts, M. S., & van Zee, L. 1998, AJ, 115, 62

Hewitt, J. N., Haynes, M. P., & Giovanelli, R. 1983, AJ, 88, 272

Impey, C. & Bothun, G. 1997, ARA&A, 35, 267

Jensen, E. B. & Thuan, T. X. 1982, ApJS, 50, 421

Jimenez, R., Padoan, P., Matteucci, F., & Heavens, A. F. 1998, MNRAS, 299, 123

Just, A., Fuchs, B., & Wielen, R. 1996, A&A, 309, 715

Karachentsev, I. 1989, AJ, 97, 1566

Karachentsev, I. 1991, Pis'ma Astron. Zh., 17, 485

Karachentsev, I. D. 1999, AstL, 25, 376

Karachentsev, I. D. & Xu, Z. 1991, Pis'ma Astron. Zh., 17, 485

Kodaira, K. & Yamashita, T. 1996, PASJ, 48, 581

Kylafis N. D. & Bahcall, J. N. 1987, ApJ, 317, 637

Lacey, C. 1991 in Dynamics of Disc Galaxies, edited by B. Sundelius, (Göteborg University and Chalmers University of Technology, Göteborg), p. 257

Landolt, A. U. 1992, AJ, 104, 340

Lin, D. N. C. & Pringle, J. E. 1987, ApJ, 320, L87

Lauberts, A. & Valentijn, E. A. 1989, The Surface Photometry Catalogue of the ESO-Uppsala Galaxies (European Southern Observatory, Garching bei München)

Lequeux, J., Fort, B., Dantel-Fort, M., Cuillandre, J.-C., & Mellier, Y. 1996, A&A, 312, L1

Makarov, D. I., Karachentsev, I. D., Tyurina, N. V., & Kaisin, S. S. 1997, AstL, 23, 445

Makarov, D. I., Karachentsev, I. D., Burenkov, A. N., Tyurina, N. V., & Korotkova, G. G. 1998, AstL, 23, 732

Matthews, L. D. 1998, Ph.D. Thesis, State University of New York at Stony Brook

Matthews, L. D. 1999, in preparation (Paper II)

Matthews, L. D. *et al.* 1999a, AJ, 118, 208

Matthews, L. D. *et al.* 1999b, in preparation

Matthews, L. D. & Gallagher, J. S. 1997, AJ, 114, 1899

Matthews, L. D. & van Driel, W. 1999, in preparation

Matthews, L. D., van Driel, W., & Gallagher, J. S. 1998, AJ, 116, 1169

McGaugh, S. S. 1994, ApJ, 426, 135

Mo, H. J., Mao, S., & White, S. D. M. 1998, MNRAS, 295, 319

Morrison, H. L., Boronson, T. A., & Harding, P. 1994, AJ, 108, 1191

Ogorodnikov, K. F. 1958, Dinamika zvezdnykh sistem (Dynamics of Stellar Systems), (Fiz. Mat. Lit., Moscow)

Olling, R. P. 1996, AJ, 112, 457

O'Neil, K., Bothun, G. D., Schombert, J., Cornell, M. E., & Impey, C. D. 1997, AJ, 114, 2448

Rice, W., Lonsdale, C. J., Soifer, B. T., Neugebauer, G., Koplan, E. L., Lloyd, L. A., de Jong, T., & Habing, H. J. 1988, ApJS, 68, 91

Roberts, M. S. & Haynes, M. P. 1994, ARA&A, 32, 115

Sage, L. J. 1993, A&A, 272, 123

Salzer, J. J., Di Serego Alighieri, S., Matteucci, F., Giovanelli, R., & Haynes, M. P. 1991, AJ, 101, 1258

Sandage, A. 1961, The Hubble Atlas of Galaxies, (Carnegie Institution of Washington, Washington)

Sasaki, T. 1987, PASJ, 39, 849

Secker, J. 1995, ApJ, 469, L81

Swaters, R. 1999, to appear in Galaxy Dynamics, ASP Conference Series, edited by D. R. Merritt, M. Valluri, and J. A. Sellwood (Astronomical Society of the Pacific, San Francisco)

Tully, R. B. 1988, Nearby Galaxies Catalog (Cambridge University Press, Cambridge)

Tully, R. B., Pierce, M. J., Huang, J.-S., Saunders, W., Verheijen, M. A. W., & Witchalls, P. L. 1998, AJ, 115, 2264

van der Hulst, J. M., Skillman, E. D., Smith, T. R., Bothun, G. D., McGaugh, S. S., & de Blok, W. J. G. 1993, AJ, 106, 548

van der Kruit, P. C. & Searle, L. 1981, A&A, 95, 105

van Zee, L., Haynes, M. P., & Giovanelli, R. 1995, AJ, 109, 990

Vorontsov-Vel'yaminov, B. 1967, in Modern Astrophysics, edited by M. Hack, p. 347

Wainscoat, R. J., Freeman, K. C., & Hyland, A. R. 1989, ApJ, 337, 163

White, S. & Frenk, C. 1991, ApJ, 379, 52

Xilouris, E. M., Byun, Y. I., Kylafis, N. D., Paleologou, E. V., & Papamastorakis, J. 1999, A&A, 344, 868

Zasov, A. V., Makarov, D. I., & Mikhailova, E. A. 1991, Sov. Astron. Lett., 12, 374

Fig. 1.— H-band image of UGC 7321 obtained with IRIM on the KPNO 2.1-m telescope. Field size is $\sim 4\farcm6 \times 1\farcm0$. East is on the right of the image, north on top. A number of foreground stars and cosmic rays have been cleaned from the image. Note the complete absence of a bulge component, even in the near-infrared.

Fig. 2.— Contour map produced from the H-band image of UGC 7321. The image has been stretched in the z direction for illustration purposes. The contours are spaced in units of 20 counts. Note the regularity of the contours, even near the galaxy center, suggesting dust absorption is minimal in the H-band.

Fig. 3.— H-band major axis profile of UGC 7321, averaged over a 3-pixel-wide strip. The axes are distance along the galaxy major axis, in arcseconds, versus the logarithm of the intensity, in arbitrary units. The arrows mark the locations of changes in slope of the brightness profile.

Fig. 4.— R-band image of UGC 7321 obtained with the WIYN telescope. Image size is $\sim 6\farcm5 \times 1\farcm0$. East is on the right, north on top. Seeing was $\sim 0\farcs6$ FWHM.

Fig. 5.— Close-up of a $1\farcm8$ long portion of the R-band WIYN image of UGC 7321. The optical center of the galaxy corresponds to the large black patch on the righthand side of the image. White areas show dust clumps in the disk. Note the absence of a true dust lane.

Fig. 6.— Close-up of the western edge of the UGC 7321 disk in the R band, showing a background galaxy visible though the disk, at approximately $2\farcm5$ west of the disk center.

Fig. 7.— Continuum-subtracted Hα image of UGC 7321 obtained with the WIYN telescope. Scale and orientation are as in Fig. 4.

Fig. 8.— Detail of the Hα emission structure centered at $\sim 8''$ east of the galaxy center. This image section is roughly $50''$ long. Note the gap in the emission at the center of this frame and the faint plumes extending out of the disk midplane.

Fig. 9.— Azimuthally-averaged B-band surface brightness profile of UGC 7321 obtained from fitting a series of 9 concentric ellipses. Axes are distance from the galaxy center in arcseconds, versus average B-band surface brightness in magnitudes per square arcsecond. The dashed line represents the best exponential fit to the data. No inclination or extinction corrections have been applied.

Fig. 10.— $B-R$ color map of the inner $3\farcm8$ of UGC 7321 obtained from our WIYN data. Seeing in both the B and R data was $\sim 0\farcs6$. Black (near the nuclear region) corresponds to $B-R \approx 1.5$; dark grey (seen surrounding the nuclear region): $B-R \approx 1.2$; mottled black and white (seen in the thicker disk surrounding the galaxy): $B-R \approx 1.1$; white (as seen along the disk major axis and in the outer disk regions): $B-R < 0.85$.

Fig. 11.— (a) $B-R$ color along the major axis of UGC 7321, averaged over a 12-pixel-wide strip.

The data have been smoothed by a factor of 15 along the r-direction. The axes are distance from the galaxy center in arcseconds versus $B-R$ color in magnitudes, corrected for Galactic foreground extinction. (b) Same as (a), but offset 1$''$.6 north of the major axis, and running through the very red nuclear feature (see Sect. 3.1). (c) Same as (a), but offset 1$''$.2 south from the major axis. (d) Same as (a), but offset 4$''$.6 south from the major axis. The very red feature near $r = -135''$ is due to a background galaxy seen through the disk.

Fig. 12.— Same as Fig. 11(a), except the profile was extracted 10$''$ north of the major axis. This cut runs through the thicker "old disk" of stars visible in Fig. 10. Note there is very little color gradient as a function of r. Beyond $r = \pm 75''$ our extracted profile no longer traces the "old disk" due to the curvature of the galaxy isophotes.

Fig. 13.— "Pseudo" $R-H$ color along the major axis of UGC 7321, in the interval $r \leq 120''$. The R data were smoothed to the H-band resolution, and the R and H intensities have been arbitrarily normalized such that $R-H \approx 0$ near r=80$''$.

Fig. 14.— (a) Same as Fig. 11(a), but with internal reddening correction applied. (b) Same as Fig. 11(b), but with internal reddening correction applied.

Fig. 15.— $B-R$ vertical color profiles extracted parallel to the minor axis of UGC 7321. The profiles are averaged over 15-pixel-wide strips and smoothed along the z direction. Axes are distance from the galaxy midplane, in arcseconds, versus $B-R$ color, corrected for Galactic foreground extinction. (a) Minor axis profile (r=0); (b) r=5$''$ east; (c) r=10$''$ east; (d) r=0$'$.5 east; (e) r=1$'$.0 east; (f) r=1$'$.25 east; (g) r=1$'$.5 east; (h) r=2$'$.0 east.

Fig. 16.— Vertical $B-R$ color profile at r=1$'$.25 east of the disk center, corrected for internal reddening. The uncorrected profile is overplotted as a dashed line.

Fig. 17.— H I pencil beam map along the major axis of UGC 7321 obtained with the Nançay Radio Telescope. The center panel shows the spectrum obtained at the optical center of the galaxy, and the remaining panels show spectra obtained at pointings offset west and east of center, respectively, at multiples of one-half beamwidth. Axes are heliocentric radial velocity, in km s$^{-1}\times 10^{-2}$, versus flux density in millijanskys.

Fig. 18.— The global H I profile of UGC 7321. Data from the seven telescope pointings shown in Fig. 17 were combined following Matthews, van Driel, & Gallagher (1998). Axes are heliocentric radial velocity, in km s^{-1}, versus flux density in millijanskys.

Fig. 19.— Rotation curve of UGC 7321 derived from the VLA H I aperture synthesis data of Rots, Roberts, & Goad (unpublished). Axes are distance along the major axis, in arcseconds, versus heliocentric radial velocity, in kilometers per second. The horizontal dashed line denotes the systemic velocity measured from our Nançay H I pencil beam measurements. The arrows indicate the edge of the stellar disk in our WIYN R-band observations, and the crosses denote the limiting

extent of the optical rotation curve derived by Goad & Roberts (1981). The close agreement between the location of V_{max} of the rotation curve and the global H I profile horns in Fig. 18 suggests are radial velocities are accurate to $\sim$10 km s^{-1}.

Fig. 20.— Schematic drawing illustrating a thin disk inclined at some angle i to the line of sight.

Fig. 21.— Blow-up of the central portion of the disk shown in Fig. 20.

This figure "fig1.gif" is available in "gif" format from:

http://arXiv.org/ps/astro-ph/9909142v1

TABLE 1. UGC 7321 Parameters

General:
$\alpha : 12^h 15^m 03^s$ (1950.0)
$\delta : +22°49'03''$ (1950.0)
Hubble type: Sd IV
Distance = 10 Mpc [a]
$A_B = 0.04$ magnitudes [b]
Measured Optical Parameters:[c]
$m_B = 13.84 \pm 0.03$
$m_R = 12.85 \pm 0.03$
$D_{opt} = 5'.6$ [d]
PA = 82°
$a/b = 10.3$ [e]
$h_r = 44'' \pm 2'' = 2.1$ kpc [f]
$\mu_B(0) = 21.6$ mag arcsec^{-2} [g]
$\mu_B(0)_{ex} = 22.0$ mag arcsec^{-2} [h]
$\bar{\mu}_B = 23.9$ mag arcsec^{-2} [i]
$B - R = 0.99$

TABLE 1. (continued)

Derived Optical Parameters:[j]
$M_B = -17.05$
$M_R = -17.70$
L_B=$1.0\times10^9 L_\odot$
$i = 88°$
A_{opt} = 16.3 kpc [k]
$\mu_{B,i}(0)$ = 23.6 mag arcsec^{-2} [l]
$\bar{\mu}_{B,i}$ = 27.6 mag arcsec^{-2} [m]
L_{FIR}/L_B=0.08 [n]
Measured HI parameters:
W_{20} = 233±7 km s^{-1}
W_{50} = 216±4 km s^{-1}
V_h = 407.2±2.2 km s^{-1}
$\int S d\nu$ = 47.6±4.0 Jy km s^{-1}
D_{HI}=7′.1 (at $N_{HI} \sim 7 \times 10^{20}$ atoms cm^{-2})
Derived HI parameters:
$\mathcal{M}_{HI} = 1.1\times10^9 M_\odot$
$\mathcal{M}_{HI}/L_B$ = 1.1 (solar units)
$D_{HI}/D_{opt} \geq$1.2

[a]From Matthews et al. (1999b)

[b]From Burstein & Heiles (1984)

[c]Observed magnitudes and luminosities have been corrected for Galactic foreground extinction only; isophotal diameters and surface brightnesses are *measured* values–i.e., uncorrected for inclination.

[d]Maximum observed angular extent of the galaxy, corresponding to the observed 25.5 mag arcsec^{-2} B-band isophote, uncorrected for inclination.

[e]Disk axial ratio measured at the observed 25.0 mag arcsec^{-2} R-band isophote.

[f]Disk scale length measured from the B-band image.

[g]Measured central surface brightness from B-band image, uncorrected for inclination and internal extinction.

[h]B-band central surface brightness obtained from extrapolation of an exponential fit to the outer disk, uncorrected for inclination and internal extinction.

[i]Mean B-band surface brightness over the observed extent of the disk, uncorrected for inclination.

[j]Derived optical quantities have been corrected for Galactic and internal extinction, as derived in Sect. 3.2.2.

[k]Linear diameter at limiting observed B-band isophote of 25.5 mag arcsec^{-2}.

[l]Predicted face-on central surface brightness, based upon the measured quantity $\mu_B(0)$.

[m]Predicted mean face-on surface brightness.

[n]Far-infrared luminosity was derived from co-added *IRAS* 100μm flux from Sage (1993) and *IRAS* 60μm flux from the NED database

This figure "fig2.gif" is available in "gif" format from:

http://arXiv.org/ps/astro-ph/9909142v1

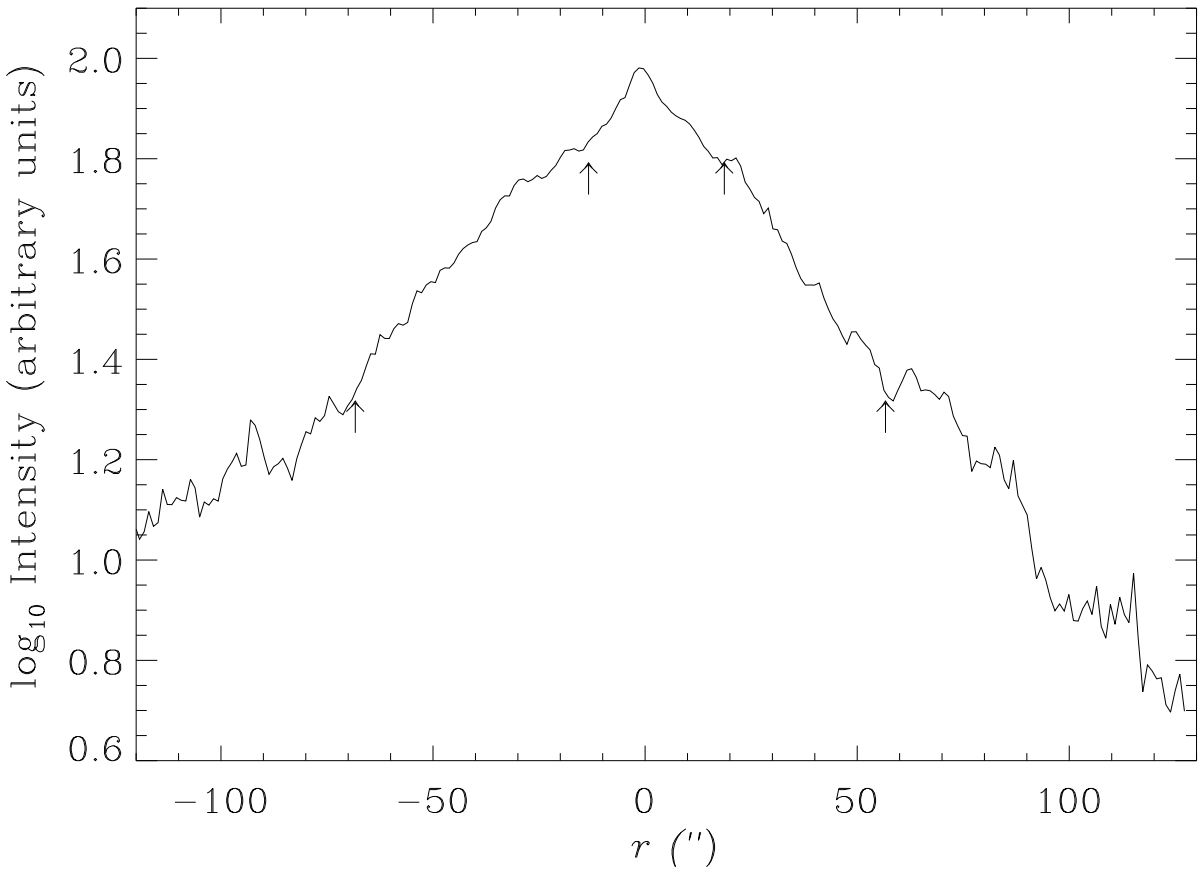
log10 Intensity (arbitrary units)
2.0
1.8
1.6
1.4
1.2
1.0
0.8
0.6
−100
−50
0
50
100
r (″)

This figure "fig4.gif" is available in "gif" format from:

http://arXiv.org/ps/astro-ph/9909142v1

This figure "fig5.gif" is available in "gif" format from:

http://arXiv.org/ps/astro-ph/9909142v1

This figure "fig6.gif" is available in "gif" format from:

http://arXiv.org/ps/astro-ph/9909142v1

This figure "fig7.gif" is available in "gif" format from:

http://arXiv.org/ps/astro-ph/9909142v1

This figure "fig8.gif" is available in "gif" format from:

http://arXiv.org/ps/astro-ph/9909142v1

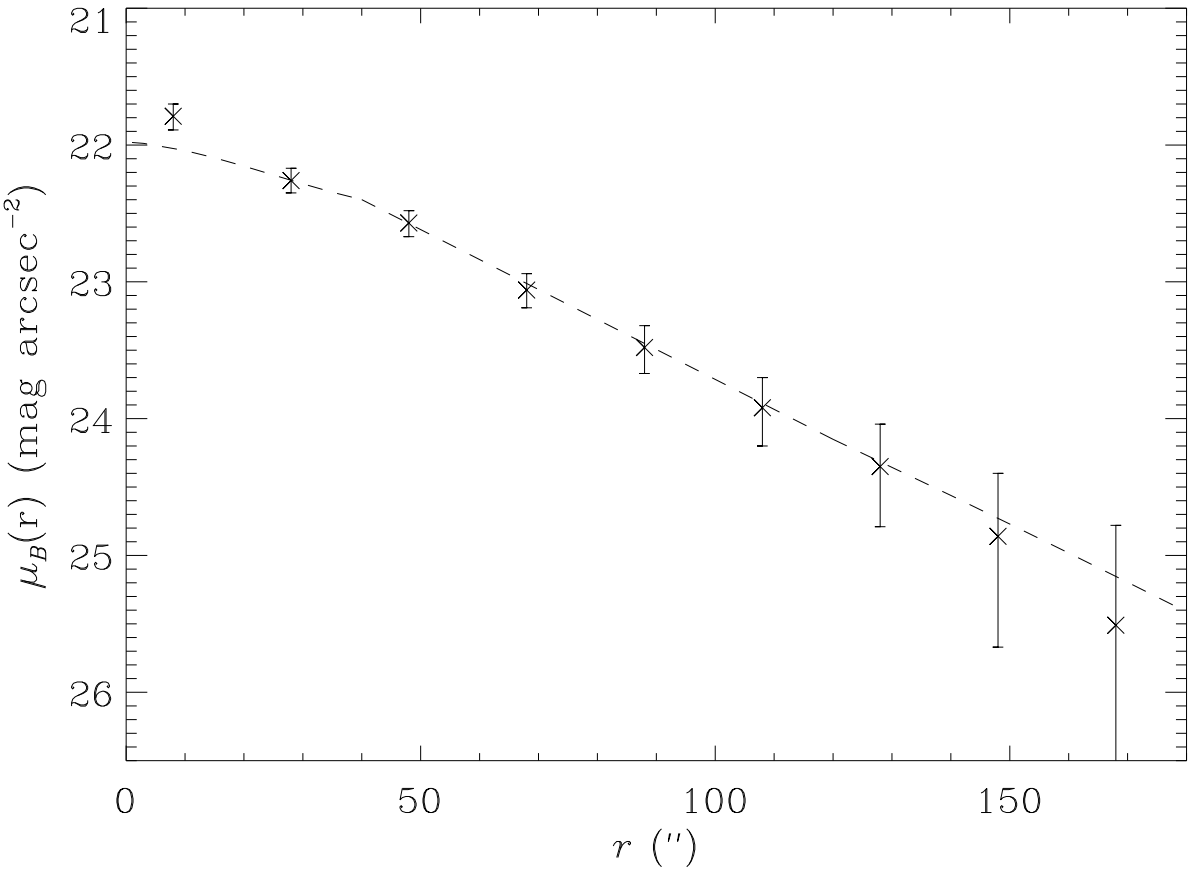
21
22
23
24
25
26
0
50
100
150
μ_B(r) (mag arcsec^{-2})
r ($''$)

This figure "fig10.gif" is available in "gif" format from:

http://arXiv.org/ps/astro-ph/9909142v1

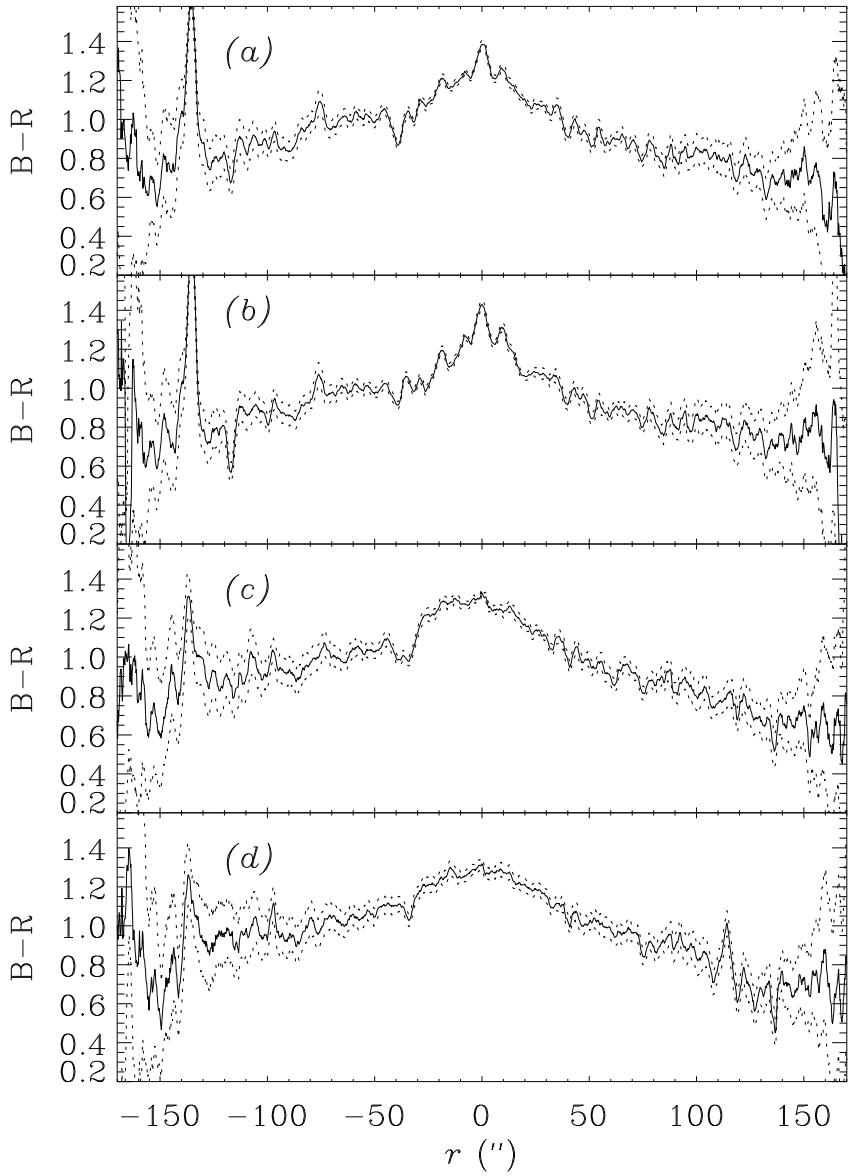
(a)
(b)
(c)
(d)
B−R
1.4
1.2
1.0
0.8
0.6
0.4
0.2
−150
−100
−50
0
50
100
150
r (″)

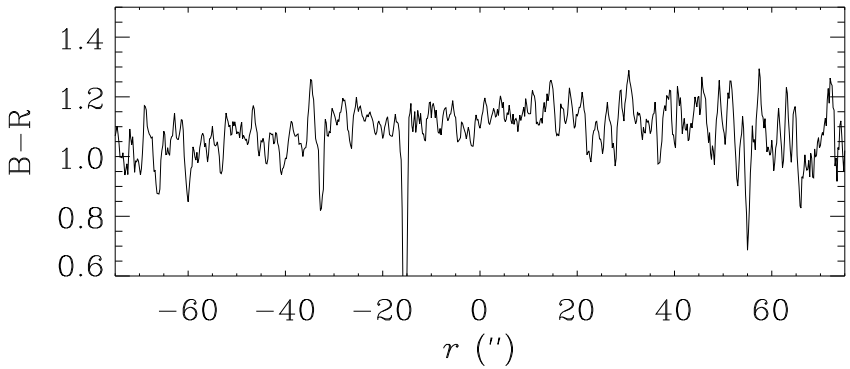
B−R
1.4
1.2
1.0
0.8
0.6
−60
−40
−20
0
20
40
60
r (″)

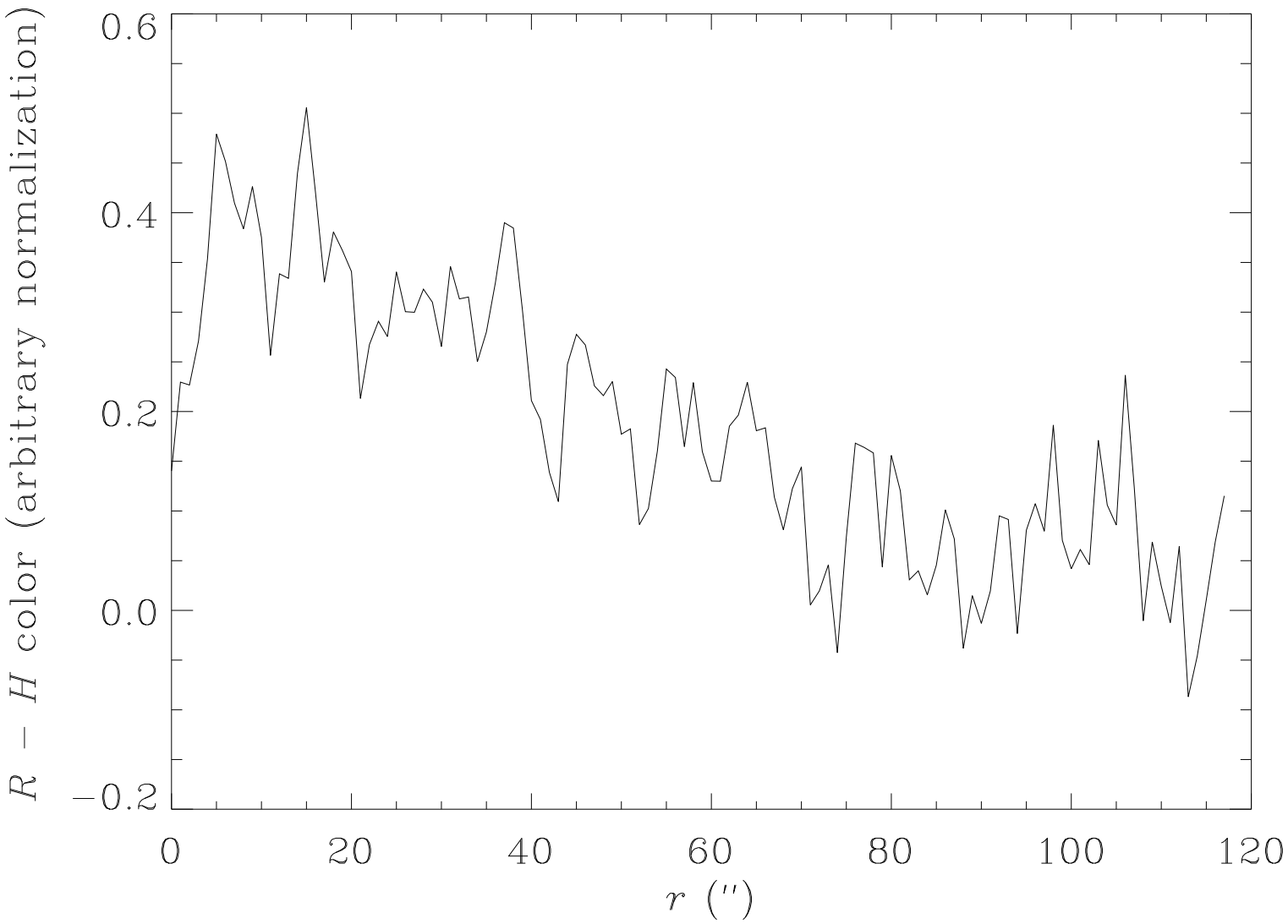
0.6
0.4
0.2
0.0
−0.2
0
20
40
60
80
100
120
$R - H$ color (arbitrary normalization)
r ($''$)

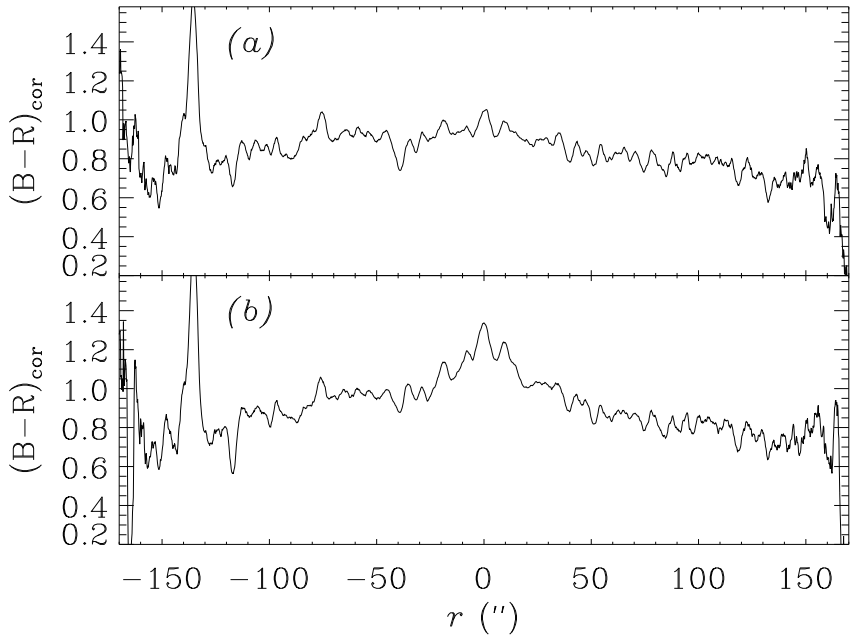
(a)
(b)
$(B-R)_{cor}$
$(B-R)_{cor}$
1.4
1.2
1.0
0.8
0.6
0.4
0.2
−150
−100
−50
0
50
100
150
r ($''$)

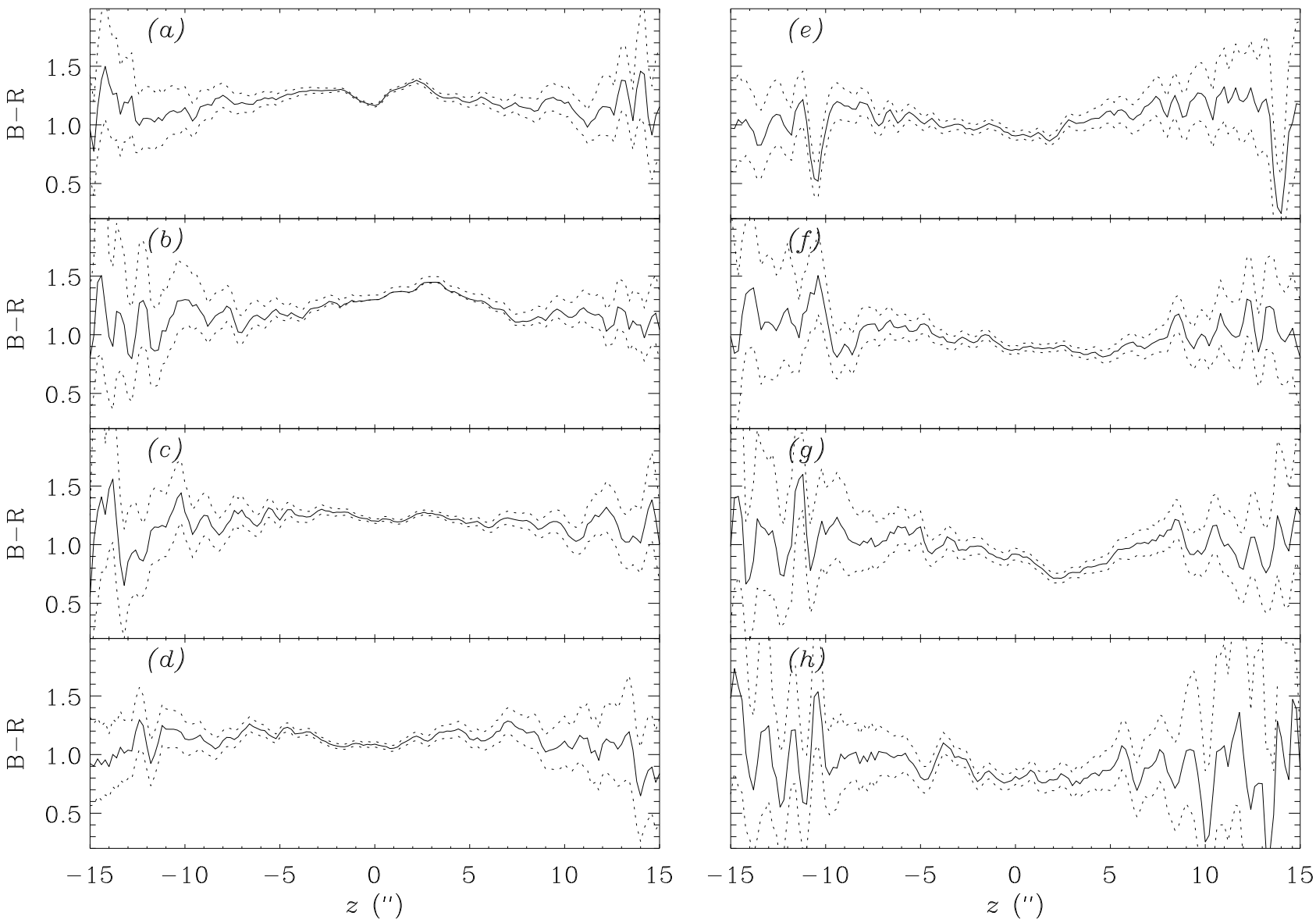
(a)
(b)
(c)
(d)
(e)
(f)
(g)
(h)
B−R
1.5
1.0
0.5
−15
−10
−5
0
5
10
15
z (″)

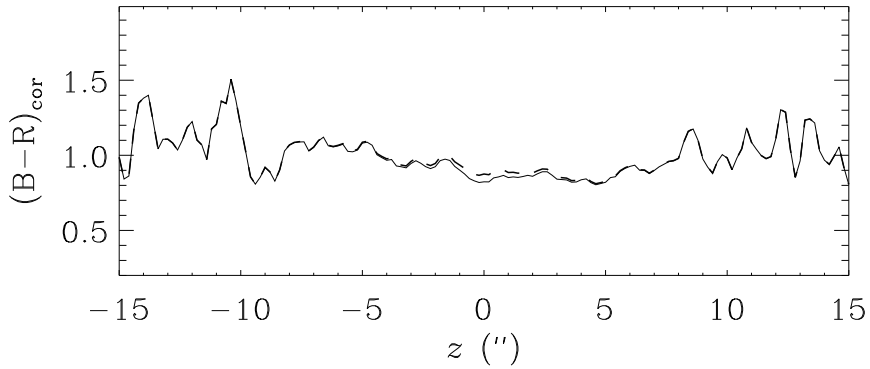
(B−R)cor
1.5
1.0
0.5
−15
−10
−5
0
5
10
15
z (″)

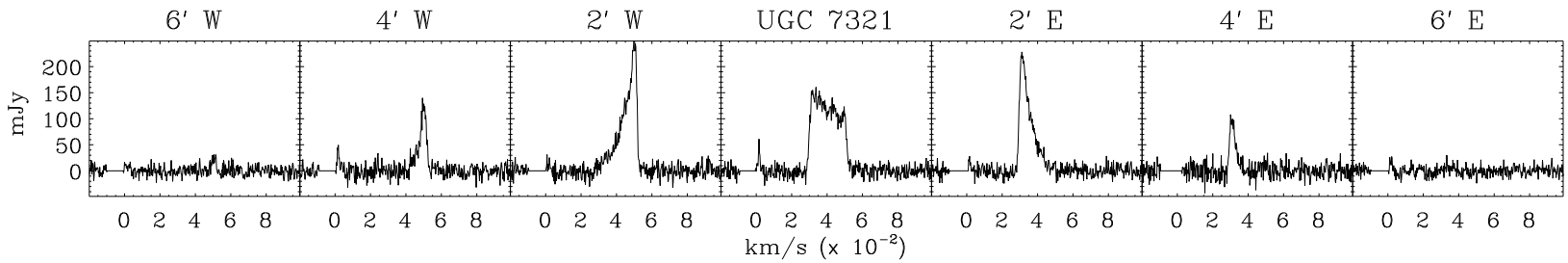
6′ W
4′ W
2′ W
UGC 7321
2′ E
4′ E
6′ E
mJy
200
150
100
50
0
0 2 4 6 8
km/s (x 10^{-2})

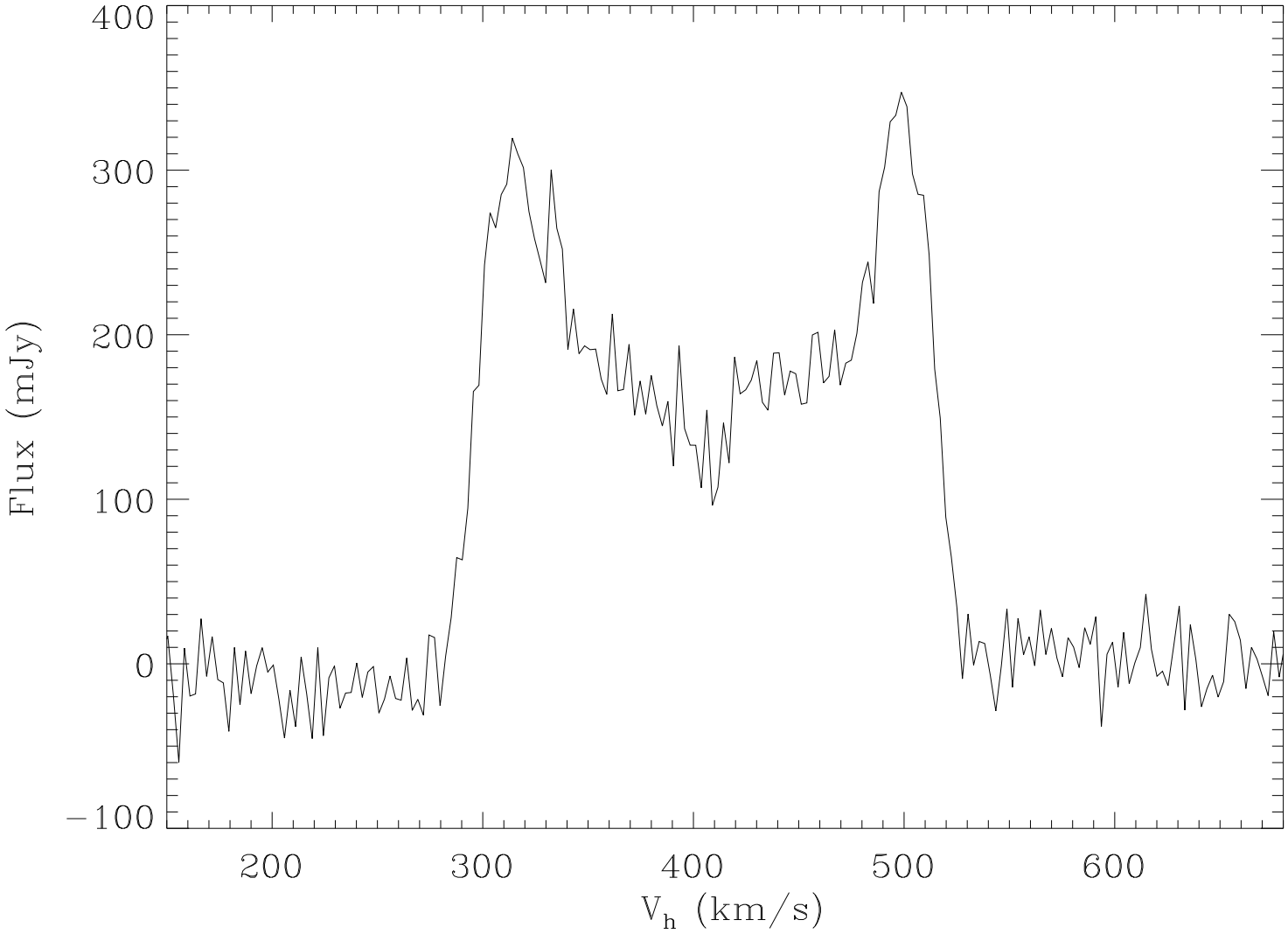
400
300
200
100
0
−100
Flux (mJy)
200
300
400
500
600
V_h (km/s)

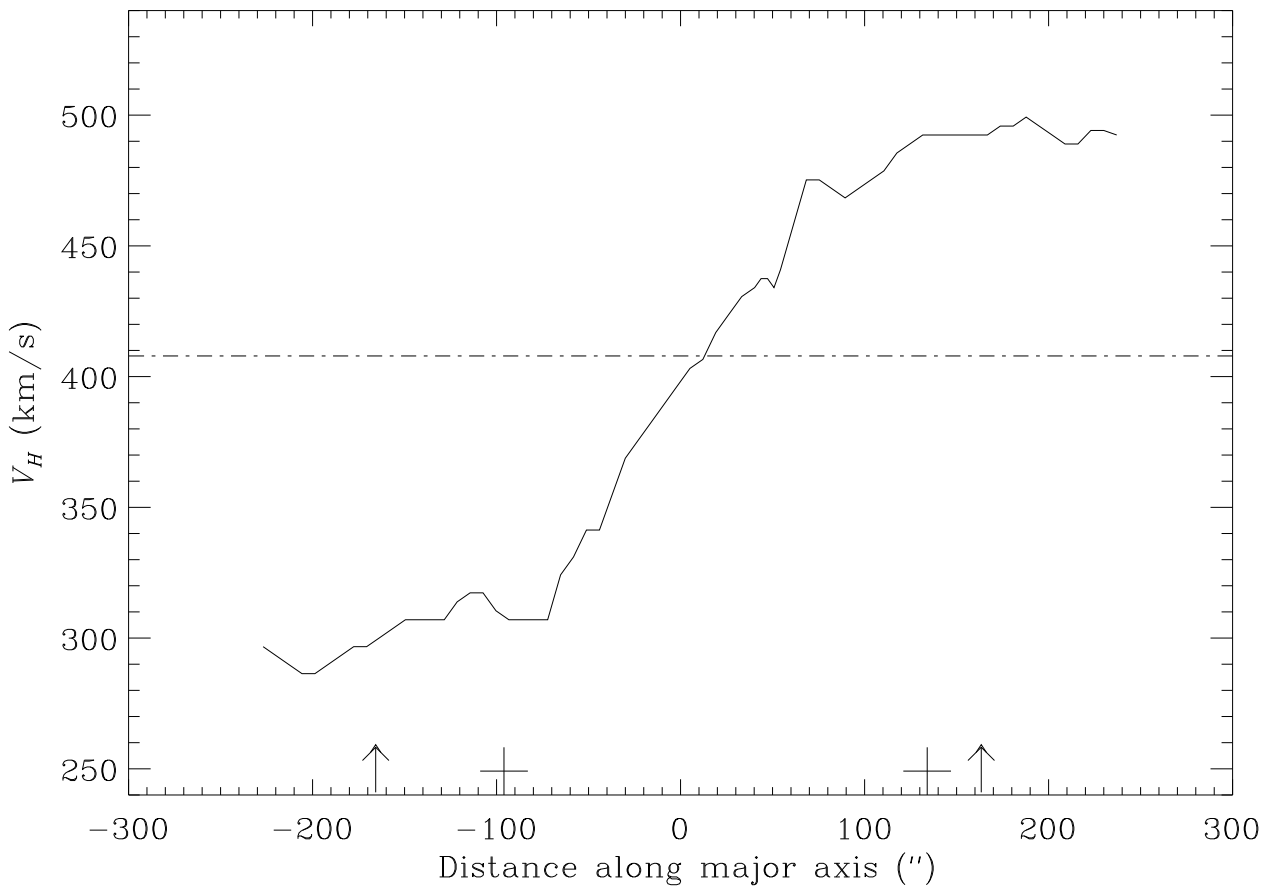
500
450
400
350
300
250
V_H (km/s)
−300
−200
−100
0
100
200
300
Distance along major axis (″)

This figure "fig20.gif" is available in "gif" format from:

http://arXiv.org/ps/astro-ph/9909142v1

This figure "fig21.gif" is available in "gif" format from:

http://arXiv.org/ps/astro-ph/9909142v1